

Improving sampling by modifying the effective diffusion

T. Lelièvre^{1,2}, R. Santet^{1,2}, G. Stoltz^{1,2}

1: CERMICS, Ecole des Ponts, Marne-la-Vallée, France

2: MATHERIALS project-team, Inria, Paris, France

October 3, 2024

Abstract

This is a preliminary version. Markov chain Monte Carlo samplers based on discretizations of (overdamped) Langevin dynamics are commonly used in the Bayesian inference and computational statistical physics literature to estimate high-dimensional integrals. One can introduce a non-constant diffusion matrix to precondition these dynamics, and recent works have optimized it in order to sooner reach stationarity by overcoming entropic and energy barriers. However, the methodology introduced to compute these optimal diffusions is not suited to high-dimensional settings, as it relies on costly optimization procedures. In this work, we propose a class of diffusion matrices, based on one-dimensional collective variables (CVs), which helps dynamics explore the latent space defined by the CV. The form of the diffusion matrix is such that the effective dynamics, which are approximations of the processes as observed on the latent space, are governed by the optimal effective diffusion coefficient in a homogenized limit, which possesses an analytical expression. We describe how this class of diffusion matrices can be constructed and learned during the simulation. We provide implementations of the Metropolis–Adjusted Langevin Algorithm and Riemann Manifold (Generalized) Hamiltonian Monte Carlo algorithms, and discuss numerical optimizations in the case when the CV depends only on a few number of components of the position of the system. We illustrate the efficiency gains of using this class of diffusion by computing mean transition durations between two configurations of a dimer in a solvent.

1 Introduction

Standard overdamped Langevin dynamics read

$$dq_t = -\nabla V(q_t)dt + \sqrt{\frac{2}{\beta}}dW_t, \quad (1)$$

where V is the potential energy function defined on the position space \mathcal{Q} of dimension d , $\beta = (k_B T)^{-1}$ is proportional to the inverse temperature (k_B is the Boltzmann constant and T is the temperature of the heat bath) and $(W_t)_{t \geq 0}$ is a standard d -dimensional Brownian Motion. Typically, $\mathcal{Q} = \mathbb{R}^{DN}$ or $\mathcal{Q} = \mathbb{T}^{DN}$ (with \mathbb{T} the one-dimensional torus) with $DN = d$, where N is the number of particles and $D \in \{1, 2, 3\}$. Under standard assumptions on the potential energy function, the process admits the Gibbs measure π as invariant measure, where π is defined by

$$\pi(dq) = Z^{-1}e^{-\beta V(q)}dq, \quad Z = \int_{\mathcal{Q}} e^{-\beta V}. \quad (2)$$

Discretizations of (1) therefore provide natural and efficient ways to sample Gibbs measures (2). One celebrated example is the Metropolis–Adjusted Langevin Algorithm (MALA) [41, 40], where the sampler is based on a Euler–Maruyama discretization of (1) along with a Metropolis–Hastings accept/reject procedure [35, 20]. This sampler achieves high performance by incorporating in the proposal the information of the derivatives of the log-density, which helps trajectories go towards

low energy regions, and therefore reach regions of high-acceptance probability, thus obtaining an efficient sampling.

Overdamped Langevin dynamics can be generalized by introducing a diffusion operator D which outputs a positive definite symmetric matrix $D(q)$ for any position q :

$$dq_t = (-D(q_t)\nabla V(q_t) + \beta^{-1} \operatorname{div} D(q_t)) dt + \sqrt{2\beta^{-1}D(q_t)}^{1/2} dW_t. \quad (3)$$

Here, the matrix $D(q_t)^{1/2}$ is the unique square root of the diffusion matrix $D(q_t)$ (defined by functional calculus) and $\operatorname{div} D(q_t)$ is defined as the vector whose i -th component is the divergence of the i -th column (or row) of the diffusion matrix $D(q_t)$. The dynamics (3) actually represent all the non-degenerate reversible diffusion processes that admit π as an invariant measure. Note that when the diffusion is set to the identity matrix for any position, the standard dynamics (1) are retrieved. The diffusion matrix D can be interpreted as the inverse of a position-dependent mass matrix, or as the inverse of a Riemannian metric. This diffusion operator acts as a preconditioner for the overdamped Langevin dynamics. It introduces multiplicative noise instead of additive noise in (1). One choice for D is the inverse of the Hessian of the potential V , provided it is definite for any position, which is the case for instance for strongly convex potentials V (as done for instance in [14, 15]).

In many practical cases of interest, target distributions are multimodal, *i.e.* regions of high probability are separated by low probability zones. This implies that local exploration methods, *e.g.* based on discretizations of (3), generate metastable trajectories: the physical system stays in one conformation for an extensive period of time (compared to the simulation time the practitioner is able to obtain numerically without prohibitive computational costs). An appropriate choice of the diffusion matrix D can yield to an efficient sampling by helping dynamics hop between modes efficiently [33].

Recent works have explored how to optimize this diffusion in order to accelerate convergence. In [9, 33], the optimizer is obtained by maximizing the spectral gap of the generator of (3). This generator writes

$$\mathcal{L} = (-D\nabla\nabla V + \beta^{-1} \operatorname{div} D) \cdot \nabla + \beta^{-1} D : \nabla^2,$$

with $:$ the Frobenius inner product and ∇^2 the Hessian operator. A more compact expression of \mathcal{L} is obtained by considering the weighted space $L^2(\pi)$:

$$\mathcal{L} = -\beta^{-1} \nabla^* D \nabla,$$

where A^* denotes the adjoint of an operator A in $L^2(\pi)$. Using this expression, one easily sees that \mathcal{L} is symmetric on $L^2(\pi)$, with smallest eigenvalue 0. The spectral gap of \mathcal{L} , denoted by Λ , is then given by the first nonzero eigenvalue. This quantity controls the convergence rate of the law of the process (3) at time t , denoted by π_t , towards the Gibbs measure (2): it holds [27, 2, 31]

$$\left\| \frac{\pi_t}{\pi} - 1 \right\|_{L^2(\pi)} \leq e^{-\beta^{-1}\Lambda t} \left\| \frac{\pi_0}{\pi} - 1 \right\|_{L^2(\pi)},$$

where we identified the probability distributions with their associated densities. Larger spectral gaps therefore lead to faster convergence towards equilibrium. The idea is then to maximize Λ with respect to D . In order for a maximization problem to be well-posed, normalization constraints need to be imposed on the diffusion. Indeed, the spectral gap associated with the diffusion αD is $\alpha\Lambda$ for any $\alpha > 0$, so that multiplying the diffusion by a large positive constant artificially increases the rate of convergence of the law of the process towards equilibrium. The catch is that, in practice, the time step has to be adapted in order to compensate for the larger variations of D . In [9], the constraint is chosen to be

$$\int_{\mathcal{Q}} \operatorname{Tr} D(q)\pi(dq) = \operatorname{Tr} \operatorname{Cov} \pi, \quad \operatorname{Cov} \pi = \mathbb{E}_\pi \left[(X - \mathbb{E}_\pi[X]) (X - \mathbb{E}_\pi[X])^\top \right] \in \mathbb{R}^{d \times d}.$$

In that case, the optimizer can be related to the so-called Stein kernels. In [33], the normalization constraint is chosen to be a variant of the L^p norm:

$$\int_{\mathcal{Q}} |D(q)|_{\mathbb{F}}^p e^{-\beta p V(q)} dq = 1. \quad (4)$$

Here, $|\cdot|_F$ denotes the Frobenius norm. An analytical expression of an optimizer can be obtained in the homogenized regime (in one dimension for the L^p constraint (4) and any dimension for linear constraints, see [33, Section 5]), which reads

$$D_{\text{Hom}}(q) = e^{\beta V(q)} \mathbf{I}_d. \quad (5)$$

The form of this diffusion has also been proposed in [39] to efficiently sampler Gibbs measures. This optimizer is also observed to be a good approximation of the optimal diffusion in one-dimensional cases [30].

It therefore seems natural to use diffusions maximizing the spectral gap of the infinitesimal generator \mathcal{L} to sample Gibbs measures. However, in high-dimensional settings, solving this optimization problem is not an easy task. For example, one way to numerically obtain the optimizers rely on Finite-Element Methods and generalized eigenvalue problems, whose costs are prohibitive in large dimensions. As for the optimal diffusion in the homogenized regime (5), the variations of the potential energy V over the potential energy surface become large in high dimension (since V is an extensive quantity), which lead to unstable dynamics.

In this work, we suggest a diffusion whose analytical expression is based on the optimal homogenized diffusion (5), where the potential energy V is replaced by an *effective* potential energy, namely the free energy F associated with a one-dimensional collective variable $\xi : \mathcal{Q} \rightarrow \mathbb{R}$. Collective variables are maps commonly used in the computational statistical physics community to describe key features of the dynamics in low dimensional subspaces. Usually, $\xi(q)$ is defined to be a slow variable of the system, that is the characteristic evolution time of $\xi(q_t)$, where q_t solves for example (1) or (3), is much larger than the characteristic time needed for the diffusion process to sample level sets of ξ . In this work, we focus on scalar-valued collective variables, the extension to the multivalued case being left for future works.

To properly introduce the class of diffusions considered in this work, let us first introduce various objects and notations. For $z \in \xi(\mathcal{Q})$, denote by $\Sigma(z) = \xi^{-1}(\{z\})$ the level set of the collective variable for the level z . The probability measure π conditioned at a fixed value z of the collective variable is given by

$$\pi^\xi(dq|z) = \frac{e^{-\beta V(q)} \|\nabla \xi(q)\|^{-1} \sigma_{\Sigma(z)}(dq)}{\int_{\Sigma(z)} e^{-\beta V} \|\nabla \xi\|^{-1} d\sigma_{\Sigma(z)}}. \quad (6)$$

The measure $\sigma_{\Sigma(z)}(dq)$ is the surface measure on $\Sigma(z)$, namely the Lebesgue measure on $\Sigma(z)$ induced by the Lebesgue measure on the ambient space \mathcal{Q} and the Euclidean product, and $\|\cdot\|$ denotes the Euclidean norm on \mathbb{R}^d . Note that the measure $\|\nabla \xi\|^{-1} d\sigma_{\Sigma(z)}$ is sometimes called the *delta measure*, denoted by $\delta_{\xi(q)-z}$. The free energy F is then given by

$$F(z) = -\beta^{-1} \ln \left(\int_{\Sigma(z)} Z^{-1} e^{-\beta V} \|\nabla \xi\|^{-1} d\sigma_{\Sigma(z)} \right), \quad (7)$$

where Z is the normalizing constant defined in (2). For any $q \in \mathcal{Q}$, we define the matrix

$$P(q) = \frac{\nabla \xi(q) \otimes \nabla \xi(q)}{\|\nabla \xi(q)\|^2} \in \mathbb{R}^{d \times d}. \quad (8)$$

For $q \in \Sigma(z)$, the orthogonal projection operator P^\perp onto the tangent space $T_q \Sigma(z)$ to $\Sigma(z)$ at q is given by (see for instance [29, Section 3.2.3.1])

$$P^\perp(q) = \mathbf{I}_d - P(q) = \mathbf{I}_d - \frac{\nabla \xi(q) \otimes \nabla \xi(q)}{\|\nabla \xi(q)\|^2}. \quad (9)$$

Note that

$$P^\perp(q) \nabla \xi(q) = 0, \quad P(q) \nabla \xi(q) = \nabla \xi(q). \quad (10)$$

Lastly, we introduce

$$\sigma^2(z) = \int_{\Sigma(z)} \|\nabla\xi\|^2 d\pi^\xi(\cdot|z). \quad (11)$$

The map σ can be seen as the (multiplicative) noise of the effective dynamics on the latent space $\xi(\mathcal{Q})$, see Section 2.1 for further details. The class of diffusions we are interested in is then defined as

$$D_\alpha(q) = \kappa_\alpha (P^\perp(q) + a_\alpha(\xi(q))P(q)) = \kappa_\alpha (\mathbf{I}_d + (a_\alpha(\xi(q)) - 1) P(q)),$$

$$\text{with } a_\alpha(z) = \frac{e^{\alpha\beta F(z)}}{\sigma^2(z)}, \quad (12)$$

where $\alpha \in \mathbb{R}$ is a numerical parameter and $\kappa_\alpha > 0$. Note that D_α defines a diffusion, in the sense that it has values in the set of symmetric positive definite matrices. Indeed, the eigenvalues of $D_\alpha(q)$ are $\kappa_\alpha > 0$ and $\kappa_\alpha(1 + a_\alpha(\xi(q)) - 1) = \kappa_\alpha a_\alpha(\xi(q)) > 0$ for any $\alpha \in \mathbb{R}$.

Let us give a brief description and motivation for the diffusion (12). Since P project vectors onto the span of $\nabla\xi$ (see (10)), the diffusion helps the system go towards new values of the collective variable by modulating the direction and amplitude of the motion along $\nabla\xi$ using the map a_α . This therefore favor sampling in directions that are “difficult to explore” (those parametrized by ξ). The analytical expression of the map a_α is based on the expression of the optimal homogenized diffusion (5). The motivation is that its form is exactly the one such that the effective dynamics observed in the latent space $\xi(\mathcal{Q})$ is governed by the optimal homogenized effective diffusion $e^{\beta F}$ (at least when $\alpha = 1$), see Section 2.1. Using this diffusion should therefore favor exploration in the latent space which, if the collective variable is well-chosen, should accelerate the convergence towards equilibrium. The factor α present in the definition of a_α is introduced to ensure that $\alpha\beta F$ is of order 1 in order to scale properly the argument in the exponential and prevent unstable dynamics in practice. Note that when $\alpha = 0$ and σ^2 is constant equal to 1, the standard overdamped Langevin dynamics (1) are retrieved. Lastly, the constant κ_α acts as (the inverse of) a normalization constant for the diffusion. When discretizing the dynamics with time step Δt , this constant simply scales the time step. In our work, since we also optimize the efficiency over Δt , it is used solely to better illustrate the efficiency gains of using (12) with $\alpha > 0$.

To construct the diffusion (12), we need two quantities that we do not know *a priori*: the free energy F defined in (7) and the effective diffusion σ^2 defined in (11). These quantities are averages with respect to conditional measures. Therefore, they can be precomputed using standard techniques estimating conditional expectations, similar to the thermodynamic integration method to estimate the mean force and free energy (see Appendix 9 and [24, 29]), or learned on the fly as will be presented in Section 2.4 where we use Adapted Biasing Force (ABF) methods [10, 23].

The particular form of the diffusion (12) is such that, when the collective variable ξ is a function of only $k \leq d$ components of q (such as for bond lengths or dihedral angles), then only those k components are modified by the diffusion. The implementation of samplers based on discretizations of overdamped Langevin dynamics can therefore be tailored to limit computational overheads, see Section 2.3 for details. Finally, relevant quantities related to the diffusion in order to run the algorithms, such as its square root, inverse and determinant, are readily available without extra computational costs, see Section 2.3.

Finally, note that this class of diffusion can also be used in samplers based on discretizations of Langevin dynamics, such as the class of (Generalized) Hamiltonian Monte Carlo ((G)HMC) algorithms [12, 21]. These algorithms add a momentum variable, generating a Markov chain in the phase space $\mathcal{Q} \times \mathbb{R}^d$. The Markov chain is constructed such that a measure $\mu(dq dp) \propto e^{-\beta H(q,p)} dq dp$, where $H : \mathcal{Q} \times \mathbb{R}^d \rightarrow \mathbb{R}$ is a Hamiltonian function, is an invariant probability measure for the Markov chain. The map H is constructed so that the marginal in position of μ is exactly π , in order for the Markov chain in position to sample the Gibbs measure (2). To introduce nonconstant diffusions in (G)HMC algorithms, the relevant framework is based on Riemann Manifold (Generalized) Hamiltonian Monte Carlo algorithms (RM(G)HMC) [14]. In that case, the diffusion acts as the inverse of a position-dependent mass tensor, which preconditions the Hamiltonian dynamics [3, 5, 4]. For good choices of the numerical parameters, these algorithms provide

a weakly consistent discretizations of the overdamped Langevin dynamics (3) [30, Section 3.3]. Since the Hamiltonian function in the RM(G)HMC algorithms is not separable, implicit problems have to be solved (*e.g.* using Newton’s method) and reversibility checks have to be implemented in order to perform an unbiased sampling [15, 36, 30]. In the case when the collective variable ξ is a function of a small number of components of q , one can optimize the implementation of Newton’s method in order to limit the computational costs (more details are given in Section 3.1.1). For our numerical example, the best results are actually obtained when using RMGHMC algorithms.

Contributions. We provide a natural way to construct good candidates for diffusions (*i.e.* leading to faster convergence towards equilibrium than when using constant diffusions) using the analytical expression (12), and describe how to implement samplers based on the overdamped Langevin dynamics (3). We also explain how the diffusion can be learned on the fly, utilizing ABF methods. Lastly, we show that it is useful to construct samplers based on discretizations of Langevin dynamics such as RM(G)HMC. In the case of a collective variable being a function of a small number of components of the position q , we detail how to tailor the samplers’ implementation in order to limit computational overheads.

Outline. In Section 2, we motivate the choice of the analytical expression of the diffusion (12) and detail how samplers based on discretizations of the overdamped Langevin dynamics (3) can be implemented. We also present an adaptive scheme to update the diffusion when the free energy and effective diffusion are not available when the simulation starts. In Section 3, we describe how the diffusion can be introduced in samplers based on discretizations of the Langevin dynamics, utilizing the RMHMC algorithm and its Generalized variant. All numerical results are presented for the same physical system composed of a dimer in a solvent, described in Section 2.3.

Assumptions on the collective variable. We assume that the collective variable is smooth (at least \mathcal{C}^2) and that the gradient of ξ is nonzero everywhere. It should be noted that the gradient and Hessian of the collective variable are needed in order to run the algorithms presented in this work. These quantities can be either derived by hand or obtained numerically using automatic differentiation tools. When the collective variable is a function of only a few components of the positions, the associated computational costs are typically negligible compared to force computations.

2 Optimizing the diffusion: the overdamped Langevin case

In this section, we make precise how the diffusion (12) can be used in combination with samplers based on discretizations of the overdamped Langevin dynamics. In Section 2.1, we provide a theoretical motivation for the diffusion (12) by computing the effective dynamics associated with the overdamped Langevin dynamics (3). We then provide in Section 2.2 one possible implementation of a sampler based on discretizations of the overdamped Langevin dynamics using the MALA algorithm. Associated numerical results are presented in Section 2.3. We next describe in Section 2.4 a methodology to learn the diffusion along the simulation, utilizing standard methods used in ABF algorithms. Associated numerical results are presented in Section 2.5.

2.1 Effective dynamics

The central motivation for the choice of the analytical expression of the diffusion (12) is that the associated effective dynamics on the latent space is governed by the optimal homogenized diffusion $e^{\beta F}$ (when $\alpha = 1$). For well-chosen collective variables, effective dynamics are good approximations of the dynamics $t \mapsto \xi(q_t)$ in the latent space $\xi(\mathcal{Q})$ [25]. In particular, whatever the map ξ , their stationary probability measure is the image of the measure π by ξ , denoted

by $\xi \star \pi(dz)$ and defined by

$$\xi \star \pi(dz) = e^{-\beta F(z)} dz = Z^{-1} \left(\int_{\Sigma(z)} e^{-\beta V} \|\nabla \xi\|^{-1} d\sigma_{\Sigma(z)} \right) dz. \quad (13)$$

Let us recall the effective dynamics obtained for the standard overdamped Langevin dynamics (1), which is derived in [25, Section 2.3]. Recall that, in our work, the collective variable ξ is a scalar-valued function.

Proposition 1. *Let q_t solve (1). Then the process $t \mapsto \xi(q_t)$ satisfies*

$$d\xi(q_t) = (-\nabla V(q_t) \cdot \nabla \xi(q_t) + \beta^{-1} \Delta \xi(q_t)) dt + \sqrt{2\beta^{-1}} \nabla \xi(q_t) \cdot dW_t.$$

The effective dynamics is defined by

$$dz_t = b(z_t) dt + \sqrt{2\beta^{-1}} \sigma(z_t) dB_t, \quad (14)$$

where

$$b(z) = \int_{\Sigma(z)} (-\nabla V \cdot \nabla \xi + \beta^{-1} \Delta \xi) d\pi^\xi(\cdot|z), \quad \sigma^2(z) = \int_{\Sigma(z)} \|\nabla \xi\|^2 d\pi^\xi(\cdot|z), \quad (15)$$

and $(B_t)_{t \geq 0}$ is a standard one-dimensional Brownian Motion. Furthermore, it holds

$$b(z) = -\sigma^2(z) F'(z) + \beta^{-1} (\sigma^2)'(z), \quad (16)$$

so that the effective dynamics can be rewritten as a one-dimensional overdamped Langevin dynamics of the form (3) with effective potential F and effective diffusion σ^2 .

In (16), the derivative of the free energy, called the *mean force*, is given by

$$F'(z) = \int_{\Sigma(z)} f d\pi^\xi(\cdot|z), \quad f = \frac{\nabla V \cdot \nabla \xi}{\|\nabla \xi\|^2} - \beta^{-1} \operatorname{div} \left(\frac{\nabla \xi}{\|\nabla \xi\|^2} \right). \quad (17)$$

The map f is called the *local mean force*. It follows from (16) that the effective dynamics (14) admits $\xi \star \pi$ as a stationary measure. The proof of the identity (16), given in [25, Lemma 2.4], is recalled in Appendix 5.

The effective dynamics (14) is governed by the effective diffusion σ^2 , which may not be optimal in order to favor exploration in the latent space $\xi(\mathcal{Q})$. It therefore makes sense to modify the diffusion of the original dynamics and thus this effective diffusion in order to obtain better convergence towards equilibrium for the effective dynamics. As the following result shows, one possible solution to modify the effective diffusion is to change the (original) diffusion only in the direction of $\nabla \xi$. The proof is given in Appendix 6.

Proposition 2. *Let q_t solve (3) with diffusion $D(q) = P^\perp(q) + a(\xi(q))P(q)$ where $a : \xi(\mathcal{Q}) \rightarrow \mathbb{R}_+^*$. Then the process $t \mapsto \xi(q_t)$ satisfies*

$$d\xi(q_t) = \left(-a(\xi(q_t)) (\nabla V(q_t) \cdot \nabla \xi(q_t) - \beta^{-1} \Delta \xi(q_t)) + \beta^{-1} a'(\xi(q_t)) \|\nabla \xi(q_t)\|^2 \right) dt \\ + \sqrt{2\beta^{-1} a(\xi(q_t))} \nabla \xi(q_t) \cdot dW_t. \quad (18)$$

The effective dynamics is then given by

$$dz_t = b_a(z_t) dt + \sqrt{2\beta^{-1}} \sigma_a(z_t) dB_t, \quad (19)$$

where

$$\begin{cases} b_a(z) = a(z)b(z) + \beta^{-1} a'(z)\sigma^2(z), \\ \sigma_a^2(z) = a(z)\sigma^2(z), \end{cases} \quad (20)$$

and $(B_t)_{t \geq 0}$ is a standard one-dimensional Brownian Motion. As in (16), the maps b_a and σ_a are related by the following identity:

$$b_a(z) = -\sigma_a^2(z) F'(z) + \beta^{-1} (\sigma_a^2)'(z). \quad (21)$$

The identity (21) shows that the probability measure $\xi \star \pi$ is still an invariant measure for the effective dynamics (18), whatever the choice of the map a . A natural candidate for the effective diffusion σ_a in (19)-(21) is the optimal homogenized diffusion $e^{\beta F}$, which was shown to be optimal in some sense in [33, Section 5]. In practice, one may want to scale the free energy by a factor $\alpha \in \mathbb{R}$ so that the argument of the exponential is not too large, thus preventing unstable dynamics. This particular choice leads to our suggestion for the diffusion (12). We demonstrate on a numerical example below that using this diffusion indeed leads to a faster exploration of the latent space, hence a better exploration of the potential energy surface.

Remark 1. *Note that any contribution of P^\perp vanishes in the evolution of the process $t \mapsto \xi(q_t)$ in (18), and subsequently in (19). There is therefore a degree of freedom corresponding to the relative contributions between P and P^\perp in the definition of the diffusion. In particular, in the case of the diffusion (12), the additive constant the free energy is defined up to has an impact on this relative contribution. An optimal choice to balance the weights between P and P^\perp is left for a future work.*

2.2 Implementation using MALA

We show how to build samplers based on discretizations of the overdamped Langevin dynamics, using MALA as an example. We also give the analytical expressions of any objects that are needed to run the algorithm, such as the inverse, determinant and divergence of the diffusion (12), see the end of this section.

MALA is built on two blocks: (i) a proposal computed using a Euler–Maruyama discretization of (3) with time step Δt and (ii) a Metropolis–Hastings accept/reject procedure [35, 20]. Even though the name MALA is usually referencing the case when $D(q) = \mathbf{I}_d$ for all $q \in \mathcal{Q}$, we also use this name when using a nonconstant diffusion. For a fixed configuration $q^n \in \mathcal{Q}$, the proposal is defined by

$$\tilde{q}^{n+1} = q^n + [-D(q^n)\nabla V(q^n) + \beta^{-1} \operatorname{div} D(q^n)] \Delta t + \sqrt{2\beta^{-1}\Delta t} D(q^n)^{1/2} G^{n+1}, \quad (22)$$

where $G^{n+1} \sim \mathcal{N}(0, \mathbf{I}_d)$. This defines the transition kernel T with density

$$T(q, q') = \left(\frac{\beta}{4\pi\Delta t} \right)^{d/2} \det(D(q))^{-1/2} \exp\left(-\frac{\beta}{4\Delta t} (q' - \mu_{\Delta t}(q))^\top D(q)^{-1} (q' - \mu_{\Delta t}(q)) \right),$$

where

$$\mu_{\Delta t}(q) = q + [-D(q)\nabla V(q) + \beta^{-1} \operatorname{div} D(q)] \Delta t.$$

MALA is described in Algorithm 1. It generates a Markov chain $(q^n)_{n \geq 0}$ which admits π as invariant measure.

Square root, divergence, inverse and determinant of the diffusion. To fully describe MALA using the class of diffusions (12), one needs to compute the square root and the divergence of the diffusion in Step [1.i], and the determinant and the inverse of the diffusion in Step [1.ii]. The particular form of the diffusion operator (12) is such that these quantities are available analytically without extra computational cost. Indeed, it is easily verified that

$$\begin{cases} D_\alpha(q)^{1/2} = \sqrt{\kappa_\alpha} \left[\mathbf{I}_d + \left(\sqrt{a_\alpha(\xi(q))} - 1 \right) P(q) \right], \\ D_\alpha(q)^{-1} = \kappa_\alpha^{-1} \left[\mathbf{I}_d + \left(\frac{1}{a_\alpha(\xi(q))} - 1 \right) P(q) \right], \\ \det D_\alpha(q) = \kappa_\alpha^d a_\alpha(\xi(q)). \end{cases} \quad (23)$$

As for the divergence, one readily checks that

$$\operatorname{div} P(q) = -\operatorname{div} P^\perp(q) = \frac{\nabla^2 \xi(q) \nabla \xi(q)}{\|\nabla \xi(q)\|^2} + \frac{\Delta \xi(q)}{\|\nabla \xi(q)\|^2} \nabla \xi(q) - 2 \frac{\nabla \xi(q)^\top \nabla^2 \xi(q) \nabla \xi(q)}{\|\nabla \xi(q)\|^4} \nabla \xi(q), \quad (24)$$

Algorithm 1 MALA.

Consider an initial condition $q^0 \in \mathcal{Q}$, and set $n = 0$.

[1.i] Compute the proposal \tilde{q}^{n+1} as in (22);

[1.ii] Draw a random variable U^n with uniform law on $[0, 1]$:

- if $U^n \leq r(q^n, \tilde{q}^{n+1})$ where

$$r(q, q') = \min \left(1, \frac{\pi(q')T(q', q)}{\pi(q)T(q, q')} \right)$$

- accept the proposal and set $q^{n+1} = \tilde{q}^{n+1}$;
- else reject the proposal and set $q^{n+1} = q^n$;

[1.iii] Increment n and go back to [1.i].

where Δ is the Laplacian operator. Besides, it holds

$$\operatorname{div}(a(\xi(q))P(q)) = a(\xi(q)) \operatorname{div} P(q) + a'(\xi(q))P(q)\nabla\xi(q) = a(\xi(q)) \operatorname{div} P(q) + a'(\xi(q))\nabla\xi(q),$$

where we used (10) for the second equality. Therefore, the divergence of the diffusion (12) is given by

$$\begin{aligned} \operatorname{div} D_\alpha(q) &= \kappa_\alpha (a_\alpha(\xi(q)) - 1) \left(\frac{\nabla^2 \xi(q) \nabla \xi(q)}{\|\nabla \xi(q)\|^2} + \frac{\Delta \xi(q)}{\|\nabla \xi(q)\|^2} \nabla \xi(q) - 2 \frac{\nabla \xi(q)^\top \nabla^2 \xi(q) \nabla \xi(q)}{\|\nabla \xi(q)\|^4} \nabla \xi(q) \right) \\ &\quad + \kappa_\alpha a'_\alpha(\xi(q)) \nabla \xi(q). \end{aligned} \tag{25}$$

Moreover, the derivative of the map a_α introduced in (12) is given by

$$a'_\alpha(z) = \frac{e^{\alpha\beta F(z)}}{\sigma^4(z)} \left[\alpha\beta F'(z)\sigma^2(z) - (\sigma^2)'(z) \right] = \frac{\beta e^{\alpha\beta F(z)}}{\sigma^4(z)} \left[(\alpha - 1)\sigma^2(z)F'(z) - b(z) \right], \tag{26}$$

where we used (16) for the second equality. The last formulation is attractive as it involves only averages with respect to conditional measures.

Remark 2. When $\|\nabla \xi\|$ is constant, which is the case for the numerical example of Section 2.3, the quantity $\nabla^2 \xi \nabla \xi$ vanishes, so that (25) simplifies as

$$\operatorname{div} D_\alpha(q) = \kappa_\alpha \left((a_\alpha(\xi(q)) - 1) \frac{\Delta \xi(q)}{\|\nabla \xi(q)\|^2} + a'(\xi(q)) \right) \nabla \xi(q).$$

Likewise, the derivative of the map a_α reduces to $a'_\alpha(z) = \alpha\beta F'(z)a_\alpha(z)$. In that case, only the free energy and the mean force are needed to construct the diffusion (12) as well as its derivatives.

To run MALA, one therefore needs to have access to the free energy (7), the mean force (17) as well as the effective drift and diffusion defined in (15). Two approaches can be undertaken to estimate these quantities:

- (i) they can be precomputed, by sampling the conditional expectations $d\pi^\xi(\cdot|z)$ using constrained sampling methods (see Appendix 9 where we detail the thermodynamic integration method for our numerical experiment);
- (ii) or learned on the fly, as will be presented below in Section 2.4.

Finally, the scalar κ_α in (12) is given by

$$\kappa_\alpha = \left(\int_{\xi(\mathcal{Q})} \sqrt{d-1+a_\alpha(z)^2} e^{-\beta F(z)} dz \right)^{-1}. \quad (27)$$

The computations leading to the formula (27) are detailed in Appendix 7. Note that the quantity κ_α simply rescales the time step Δt when discretizing the overdamped Langevin dynamics. It is therefore not strictly necessary to compute it in order to run the MALA algorithm. In particular, in the numerical experiments of Section 2.3, we optimize over the time step Δt for each value of α , so that computing κ_α is only performed in order to obtain similar optimal time steps. However, the computation of κ_α becomes relevant when learning the free energy F on the fly (as described in Section 2.4), in order to properly scale the updated values of the diffusion with respect to the time step Δt and prevent unstable dynamics.

2.3 MALA: numerical results

We illustrate the sampling efficiency gains when discretizing overdamped Langevin dynamics (3) with diffusion (12), utilizing the MALA algorithm described in Algorithm 1. The system we consider has been used as a toy model for sampling reactive trajectories, typically between two geometric configurations of a protein, see [29] and references therein.

Physical system. We consider a two-dimensional system composed of $N = 16$ particles (hence $d = 2N$) interacting through the following repulsive WCA pair potential:

$$V_{\text{WCA}}(r) = \begin{cases} 4\varepsilon \left[\left(\frac{R}{r} \right)^{12} - \left(\frac{R}{r} \right)^6 \right] + \varepsilon & \text{if } r \leq r_0, \\ 0 & \text{if } r > r_0. \end{cases}$$

Here, r denotes the distance between two particles, $\varepsilon = 1$ and $R = 1$ are two positive parameters and $r_0 = 2^{1/6}R$. Two particles are designated to form a solute dimer while the others are solvent particles. For these two particles, the WCA potential is replaced by the following double-well potential

$$V_{\text{DW}}(r) = h \left(1 - \frac{(r - r_0 - w)^2}{w^2} \right)^2. \quad (28)$$

This potential admits two minima, one corresponding to the compact state $r = r_0$, and one corresponding to the stretched state $r = r_0 + 2w$ with $w = 0.7$. The energy barrier separating both states is $h = 2$. The particles are placed in a periodic square box with side length ℓ such that the particle density is $N/\ell^2 = 0.7$ (thus $\ell \approx 4.78$). We set $\beta = 1$.

To fix the notations, we denote by $q = (q_1, \dots, q_N) \in (\ell\mathbb{T})^{2N}$ the positions of the system, with q_1 and q_2 forming the dimer. The potential energy function considered therefore writes

$$V(q) = V_{\text{DW}}(\|q_2 - q_1\|) + \sum_{\substack{i \in \{1,2\} \\ 3 \leq j \leq N}} V_{\text{WCA}}(\|q_i - q_j\|) + \sum_{3 \leq i < j \leq N} V_{\text{WCA}}(\|q_i - q_j\|). \quad (29)$$

Note that the distances appearing in (29) are computed taking the periodic boundary conditions into account.

Collective variable. The collective variable ξ is defined by

$$\xi(q) = \frac{\|q_2 - q_1\| - r_0}{2w}.$$

The value of the collective variable is 0 when the dimer is in a compact state, and 1 when it is in a stretched state. We therefore define two subsets of the configuration space that correspond to these two metastable states:

$$C_0 = \xi^{-1}(-\infty, \eta), \quad C_1 = \xi^{-1}(1 - \eta, +\infty), \quad (30)$$

where $\eta = 0.1$ is a numerical parameter that sets a tolerance to identify the two states. The latent space $\xi(\mathcal{Q})$ is approximated by the interval $[z_{\min}, z_{\max}] = [-0.2, 1.225]$ (which is the range of values of the collective variable observed during test runs).

Note that the collective variable is a function of only the first two particles of this two-dimensional system, meaning that its derivatives vanish for components other than the first four. In fact, it holds

$$\nabla \xi(q) = \frac{1}{2w \|q_2 - q_1\|} \begin{pmatrix} x_1 - x_2 \\ y_1 - y_2 \\ -(x_1 - x_2) \\ -(y_1 - y_2) \\ 0 \\ \vdots \\ 0 \end{pmatrix} \in \mathbb{R}^{2N}. \quad (31)$$

Diffusion. Since the collective variable $\xi(q)$ is related to a bond length, the map σ defined in (15) is constant, and is simply equal to (see (31))

$$\|\nabla \xi\|^2 = \frac{1}{2w^2} \approx 1.0204.$$

In the numerical experiments, we simply choose $\sigma = 1$ (instead of $1/(2w^2)$) which can be seen as a slight modification of (12) by adding a multiplicative constant in the definition of a_α , see Remark 1. This implies that the standard dynamics with constant diffusion is obtained by setting $\alpha = 0$. We can also use the simplifications described in Remark 2. The numerical parameter $\alpha \geq 0$ appearing in (12) should typically be chosen such that $\alpha \beta F \circ \xi$ is of order 1 over $[z_{\min}, z_{\max}]$ to reduce numerical instabilities. In our numerical setting, the variations of F are of order h over this interval, so that α should be of order $1/(\beta h)$. We use a left-Riemann rule to approximate the value of κ_α defined by (27).

Optimization in the implementation of MALA. Since ξ is a function of only 4 components, the additional computations and storage (compared to the standard MALA algorithm with identity diffusion) is limited as the diffusion (12) is block diagonal, with a 4×4 block followed by a scalar $(2N - 4) \times (2N - 4)$ matrix which does not depend on the position. More precisely,

$$D_\alpha(q) = \kappa_\alpha \begin{pmatrix} \mathbb{I}_4 + (a_\alpha(\xi(q)) - 1)\tilde{D}(q) & 0_{4,2N-4} \\ 0_{2N-4,4} & \mathbb{I}_{2N-4} \end{pmatrix} \in \mathbb{R}^{2N \times 2N}, \quad (32)$$

with

$$\tilde{D}(q) = \frac{1}{2} \begin{pmatrix} A(q) & -A(q) \\ -A(q) & A(q) \end{pmatrix} \in \mathbb{R}^{4 \times 4}, \quad A(q) = \frac{q_1 - q_2}{\|q_1 - q_2\|} \otimes \frac{q_1 - q_2}{\|q_1 - q_2\|} \in \mathbb{R}^{2 \times 2}.$$

Additionally, this means that

- the gradient of ξ has at most 4 nonzero components (see (31)), and the only nonzero part of the Hessian of ξ is a 4×4 submatrix. In fact, for our numerical example, the gradient of ξ only has two degrees of freedom while its Hessian only has three, thanks to the relations between the various derivatives of ξ in (31) (and in (57), see Appendix 8);
- the divergence of the diffusion (25) only acts through derivatives of ξ , so that only its first four components can be nonzero. In fact, for our numerical experiment, the divergence only has two degrees of freedom (see (58) in Appendix 8).

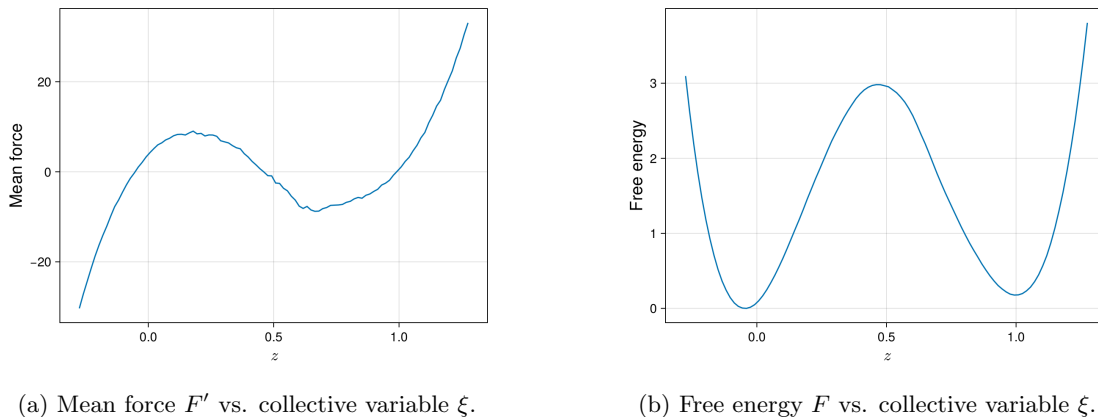


Figure 1: Mean force and free energy computed with thermodynamic integration.

Therefore, only the update related to the first two particles is notably modified compared to the standard case $D = I_d$. These observations can be generalized to any collective variable which is a function of only $k \leq d$ components of the positions.

Setting of the numerical experiment. When sampling Gibbs measures (2), one waits for the dynamics to reach the stationary state before computing various statistics. We therefore assume that the free energy F and mean force F' have been fully learned (see Section 2.4 where we explain how to learn these quantities on the fly). To estimate F' (and recover F), we used thermodynamic integration as described in Appendix 9. The mean force and the free energy obtained with this procedure are plotted in Figures 1a and 1b, respectively. Observe that the free energy well associated with the compact state is lower than the one corresponding to the stretched state, which means that the compact state is more likely than the stretched one. The free energy is defined up to an additive constant: we fix this constant so that the minimum of the free energy over the interval $[z_{\min}, z_{\max}]$ is 0. We therefore deviate from the definition given in (7), and the quantity $e^{-\beta F(z)}$ does not normalize to 1 on $\xi(\mathcal{Q})$. Note that this does not impact the form of the optimal homogenized effective diffusion, but only alters the definition of a_α by introducing a multiplicative constant, see Remark 1.

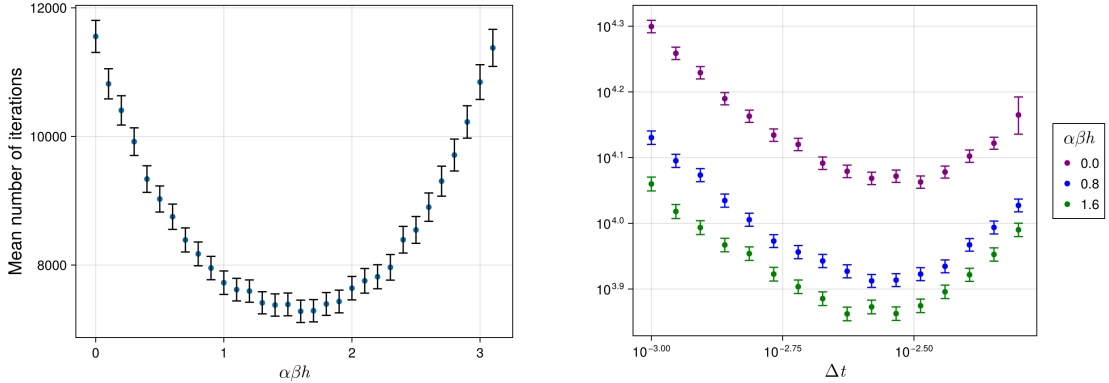
Efficiency metric. To observe the efficiency of using nonconstant diffusion matrices, we compute the mean number of iterations to go back and forth from one metastable state to the other. More precisely, we consider the initial condition $q^0 = (q_1^0, \dots, q_N^0) \in (\ell\mathbb{T})^{2N}$ defined by

$$\forall 1 \leq i \leq N, \quad q_i^0 = (x_i^0, y_i^0), \quad \begin{cases} x_i^0 = a(0.5 + \lfloor (i-1)/4 \rfloor) \\ y_i^0 = a(0.5 + ((i-1) \bmod 4)), \end{cases} \quad (33)$$

where $a = \ell/\sqrt{N} \approx 1.20$, except for y_2^0 which is set to $y_1^0 + r_0$ so that $\xi(q^0) = 0$. This particular configuration is such that the dimer is in a compact state, *i.e.* $\xi(q^0) = 0$, and the other particles are initially set on a lattice. We introduce the additional variable $\Theta^0 = 0$. This additional variable keeps track of whether the dimer last visited the compact (0) or the stretched (1) state. We define the following stopping times and values of the additional variable: $\tau^0 = 0$, and

$$\tau^{k+1} = \min_{n \geq 1} \left\{ q^{n + \sum_{i=1}^k \tau^i} \in C_{\Theta^{k+1}} \right\}, \quad \Theta^{k+1} = 1 - \Theta^k,$$

where the sets C_0, C_1 are defined in (30). Each value τ^i corresponds to the number of iterations of the dynamics used to transition between C_0 to C_1 or C_1 to C_0 , depending on the parity of i .



(a) Minimum values over the range of time steps for each value of α .

(b) Mean number of iterations as a function of Δt for some values of α .

Figure 2: Sampling efficiency using the MALA algorithm 1.

The simulation is run until $K = 10^5$ transitions are observed. The mean number of iterations for a given value of α and time step Δt is then estimated as

$$\hat{\tau}(\alpha, \Delta t) = \frac{1}{K} \sum_{k=1}^K \tau^k.$$

We denote by $\hat{\tau}(\alpha)^*$ the minimum value of $\hat{\tau}(\alpha, \cdot)$ over the range of time steps Δt used in this numerical experiment.

To perform the numerical experiment, we choose 16 values of the time step evenly spaced log-wise in the interval $[10^{-3}, 5 \times 10^{-3}]$. We present the results for values of α such that

$$\alpha\beta h \in \{0, 0.1, 0.2, \dots, 3.1\}.$$

For larger values of $\alpha\beta h$, the mean number of iterations dramatically increase, and eventually the numerical scheme becomes unstable (we observe numerical overflows for $\alpha\beta h \geq 4.2$ for the time steps we consider). This could be fixed by imposing an upper bound on the diffusion.

Results. We present in Figure 2 the mean number of iterations as a function of the time step Δt for various values of α . The error bars represent 95% confidence intervals. The minimal number of iterations across all simulations is obtained for $\alpha_{\text{opt}}\beta h = 1.6$, *i.e.* $\alpha_{\text{opt}} = 0.8$. For this value, it holds $\hat{\tau}(\alpha_{\text{opt}})^* = 7281$, while $\hat{\tau}(0)^* = 11556$. This shows that using $\alpha > 0$, thus introducing multiplicative noise with the diffusion (12), is useful to cross energy barriers, thus enhancing the exploration efficiency of the configuration space. Figure 2a shows the behavior of $\alpha \mapsto \hat{\tau}(\alpha)^*$. The minimum values were all obtained for time steps which were similar, around $\Delta t \approx 2.6 \times 10^{-3}$ (thanks to the normalization of the diffusion). Figure 2b shows that, when $\hat{\tau}(\alpha_1)^* \leq \hat{\tau}(\alpha_2)^*$ for two values of $\alpha \in \{\alpha_1, \alpha_2\}$, then $\hat{\tau}(\alpha_1, \Delta t) \leq \hat{\tau}(\alpha_2, \Delta t)$ for any time step Δt used in this numerical experiment. This means that any value of α such that $\alpha\beta h \in (0, 3.1)$ can be used to obtain better performance, regardless of the time step used. Finally, note that for small time steps, the mean number of iterations scales as Δt^{-1} . This is consistent with the fact that MALA is a weakly consistent discretization of the overdamped Langevin dynamics (3), so that the simulation time t_{sim} is simply related to the number of iterations N_{iter} and the time step Δt as $t_{\text{sim}} = N_{\text{iter}}\Delta t$.

2.4 Adaptive learning of the diffusion

When the free energy (7), the mean force (17), or the effective drift and diffusion (15) are not available at startup, they can be learned during the simulation as is done in Adapted Biasing Force

(ABF) methods [10, 23]. These methods are used to compute free energy differences between metastable states, *i.e.* relative likelihood of states. Standard dynamics such as (1) are modified by adding a force which biases the dynamics towards unexplored regions. This additional force is an estimate of the mean force F' , which is learned on the fly, and the bias is updated in order for the dynamics to escape metastable states.

Actually, ABF methods simply rely on the update of conditional expectations with respect to π^ξ (see (6)). The diffusion (12) depends on these conditional expectations, through the effective diffusion function σ and free energy F (recovered by integrating the mean force F'). The divergence of the diffusion, whose analytical expression is given in (25), also requires to compute such conditional expectations for some specific observables. We can therefore learn these quantities when performing the simulation, and update the diffusion (and its divergence) while still obtaining an (almost) unbiased sampling of the target probability distribution (2). Let us make precise one way to approximate expectations with respect to the conditional measure π^ξ defined in (6). We refer to [29, Section 5.1.3] for general discretization methods to approximate these quantities.

Let q_t solves the overdamped Langevin dynamics (3). To compute a conditional expectation of the form

$$\int_{\Sigma(z)} h \, d\pi^\xi(\cdot|z), \quad (34)$$

where $h : \mathcal{Q} \rightarrow \mathbb{R}$, the idea is to update values of a map $\Gamma_t(z)$ along the simulation (where t represents the simulation time) in order for $\Gamma_t(z)$ to converge to (34) in the long time limit. To naturally construct these maps, we rely on the formal identity

$$\int_{\Sigma(z)} h \, d\pi^\xi(\cdot|z) = \lim_{\Delta z \rightarrow 0} \frac{\mathbb{E} [h(q_t) \mathbb{1}_{\{\xi(q_t) \in (z, z + \Delta z)\}}]}{\mathbb{P}(\xi(q_t) \in (z, z + \Delta z))}.$$

Both the numerator and denominator can be approximated using empirical averages over a trajectory and/or multiple replicas, introducing a binning of the collective variable values to get a piecewise constant (in z) approximation. This is made precise in the next paragraph.

The discretization in practice. We now specify the methodology used in the numerical experiments. Let us consider an interval $[z_{\min}, z_{\max}]$ of the latent space $\xi(\mathcal{Q})$ over which the diffusion will be approximated. Outside this interval, the diffusion will simply set to a constant. The interval $[z_{\min}, z_{\max}]$ should be chosen so that most of the values of the collective variable lie in it. We next discretize this interval using N_z bins by defining

$$z^i = z_{\min} + i\Delta z, \quad \Delta z = \frac{z_{\max} - z_{\min}}{N_z}.$$

We thus construct an approximation of the map Γ_t using a piecewise constant map on $[z_{\min}, z_{\max}]$. Denote by $(q^k)_{0 \leq k \leq N}$ a trajectory obtained from a discretization of (3) (*e.g.* using MALA). The value of $\Gamma_t(z)$ at time $t_n = n\Delta t$ is then approximated as

$$\Gamma_{n\Delta t}^{\Delta z} \left(\left\lfloor \frac{z - z_{\min}}{\Delta z} \right\rfloor \right), \quad \Gamma_{n\Delta t}^{\Delta z}(i) = \frac{\sum_{j=0}^n h(q^j) \mathbb{1}_{\{\xi(q^j) \in (z^i, z^{i+1})\}}}{\sum_{j=0}^n \mathbb{1}_{\{\xi(q^j) \in (z^i, z^{i+1})\}}}. \quad (35)$$

Hyperparameters. ABF methods usually use additional hyperparameters, which prevent numerical instabilities when discretizing the dynamics. We consider two of them here:

- The learned diffusion is used in a given bin only if this bin has been visited a sufficiently large number of times, the threshold being given by N_{\min} .
- The update of the conditional expectation is done every N_{update} steps of the dynamics.

Conditional expectations computed for the diffusion (12). Two conditional expectations are needed for the diffusion (12): one related to σ^2 defined by (15), and one related to the mean force F' defined by (17). Note that when $\|\nabla\xi\|$ is constant, one only needs to approximate the mean force, and that the scalar κ_α appearing in (12) also relies on the free energy, see Appendix 7.

When approximating the mean force F' (respectively the effective diffusion function σ), we choose 0 (respectively 1) as the value used for the mean force (respectively the effective diffusion) when there are not enough observations in a bin or when the value of the collective variable is outside the interval $[z_{\min}, z_{\max}]$.

To approximate the values of the free energy F , we simply integrate the approximation of the mean force over the interval $[z_{\min}, z_{\max}]$. The values of the free energy outside the mesh are set in order to obtain a continuous function. Lastly, we fix the additive constant of the free energy so that the minimum value of the free energy over the interval $[z_{\min}, z_{\max}]$ is 0.

Conditional expectations computed for the divergence of the diffusion (12). In view of (25)-(26), the effective drift b defined in (15) also needs to be approximated, using similar strategies as for the mean force F' (actually, the mean force and effective drift b are opposite one another when $\|\nabla\xi\|$ is constant and equal to 1, see (16)). Note that the identity (21) therefore does not hold in this discretized setting (we still perform a Metropolis–Hastings accept/reject procedure to ensure that the Gibbs measure is sampled accordingly).

Normalization constant of the diffusion. Finally, note that the normalization constant of the diffusion varies along the simulation, as it depends on the free energy F and the effective diffusion function σ , see (27).

Adaptive MALA. We are now in position to describe the adaptive MALA algorithm, see Algorithm 2. The symbols $(F'_{n\Delta t})'$, $F'_{n\Delta t}$, $\sigma_{n\Delta t}$, $b_{n\Delta t}$, which are maps/vectors defined on $\{0, N_z - 1\}$ with values in \mathbb{R} , should be understood as the approximations at time $n\Delta t$ (*i.e.* iteration n) of the mean force (17), free energy (7) and effective diffusion and drift functions (15) respectively. The symbols $\kappa_{\alpha, n\Delta t}$, $D_{\alpha, n\Delta t}$ should be understood as the current approximation of the normalization constant of the diffusion (see (27)) and the diffusion (see (12)) respectively.

Note that Algorithm 2 belongs in the class of adaptive MCMC algorithms (see for instance [17, 18, 38]). It is therefore not clear that the Gibbs measure π is correctly sampled, even though each iteration yields a kernel which is reversible with respect to π . A sufficient condition to ensure unbiased sampling in the long-time limit is that all the quantities learned over the simulation eventually converge, see [37, Theorem 1]. Proving that these methods actually converge is usually not straightforward, as was noted for the long-time convergence of ABF methods, see for instance [28, 26, 7, 8, 1, 13].

Of course, one can stop the learning process at any iteration, and plug the learned quantities in Algorithm 1, which will ensure an unbiased sampling. The convergence of these quantities is usually observed to be rather fast in most numerical applications (compared to the total number of iterations the practitioner uses), which limits the bias. This will be illustrated in Section 2.5 using our numerical experiments.

2.5 Adaptive MALA: numerical results

The numerical experiment is the same as in Section 2.3: the only difference is that the scheme used is Adaptive MALA instead of MALA. Since $\|\nabla\xi\|$ is constant, we only need to learn the mean force F' . We set $N_{\min} = 100$ and $N_{\text{update}} = 20$. The current approximation of the scalar κ_α is simply computed by using a left-Riemann rule every time the free energy and effective diffusion get updated.

We present the results in Figure 2. We obtain $\hat{\tau}(\alpha_{\text{opt}})^* = 7306$ for $\alpha_{\text{opt}} = 0.8$ while $\hat{\tau}(0)^* = 11577$. The comments on the results are the same as the ones of Section 2.3. This shows that the same efficiency is obtained with the adaptive scheme. This is expected, as the learned quantities

Algorithm 2 Adaptive MALA.

Consider an initial condition $q^0 \in \mathcal{Q}$, and set $n = 0$. Additionally, set

$$\left\{ \begin{array}{l} \left((F_0^{\Delta z})' (i) \right)_{0 \leq i \leq N_z - 1} = 0, \\ (F_0^{\Delta z} (i))_{0 \leq i \leq N_z - 1} = 0, \\ (b_0^{\Delta z} (i))_{0 \leq i \leq N_z - 1} = 0, \\ (\sigma_0^{\Delta z} (i))_{0 \leq i \leq N_z - 1} = (1)_{0 \leq i \leq N_z - 1}, \\ \kappa_{\alpha, 0}^{\Delta z} = 1. \end{array} \right.$$

[2.i] Perform one step of the MALA algorithm 1 using the diffusion

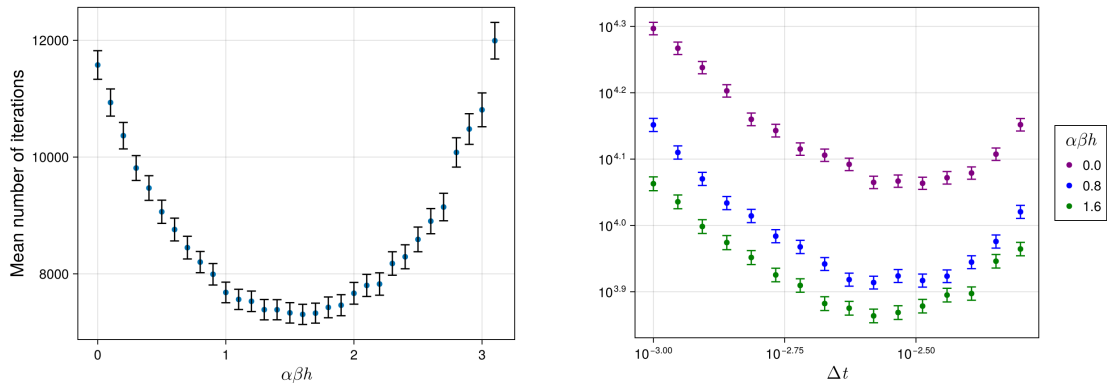
$$D_{\alpha, n\Delta t}^{\Delta z} (q) = \kappa_{\alpha, n\Delta t}^{\Delta z} (P^\perp (q) + a_{\alpha, n\Delta t}^{\Delta z} (\xi(q)) P(q)), \quad a_{\alpha, n\Delta t}^{\Delta z} (z) = \frac{e^{\alpha \beta F_{n\Delta t}^{\Delta z} (z)}}{(\sigma_{n\Delta t}^{\Delta z})^2 (z)}.$$

The divergence of the diffusion is approximated using (25) where κ_α, F, F', b and σ are replaced by their current approximations.

[2.ii] Increment n . Store the values of the local mean force f (see (17)), of the integrand of b (see (15)), and of $\|\nabla \xi\|^2$. Update the histogram of the collective variable values. If $n \equiv 0 \pmod{N_{\text{update}}}$:

- (a) Update the effective drift $b_{n\Delta t}^{\Delta z}$, effective diffusion $\sigma_{n\Delta t}^{\Delta z}$ and the mean force $(F_{n\Delta t}^{\Delta z})'$ using the formulas (35), while considering the additional rules related to N_{min} and the histogram values in each bin;
- (b) Update the free energy $F_{n\Delta t}^{\Delta z}$;
- (c) Update the normalization constant $\kappa_{\alpha, n\Delta t}^{\Delta z}$.

[2.iii] Go back to [2.i].



(a) Minimum values over the range of time steps for each value of α .

(b) Mean number of iterations as a function of Δt for some values of α .

Figure 3: Sampling efficiency using the Adaptive MALA algorithm 2.

usually only need a small number to be converged. This is depicted in Figure 4: we run a sample trajectory using 6×10^4 iterations with time step $\Delta t = 2.6 \times 10^{-3}$ and $\alpha = 0$ (we checked that similar results were obtained using other values of α). Looking at Figure 3, we should see about 5 transitions on average. We plot in Figure 4a the values of the reaction coordinate as a function of the number of iterations, and observe that 5 transitions occur (the last one happening when stopping the simulation). We present in Figure 4b the values of the free energy over the range $[z_{\min}, z_{\max}]$ for 5 values of the number of iterations n :

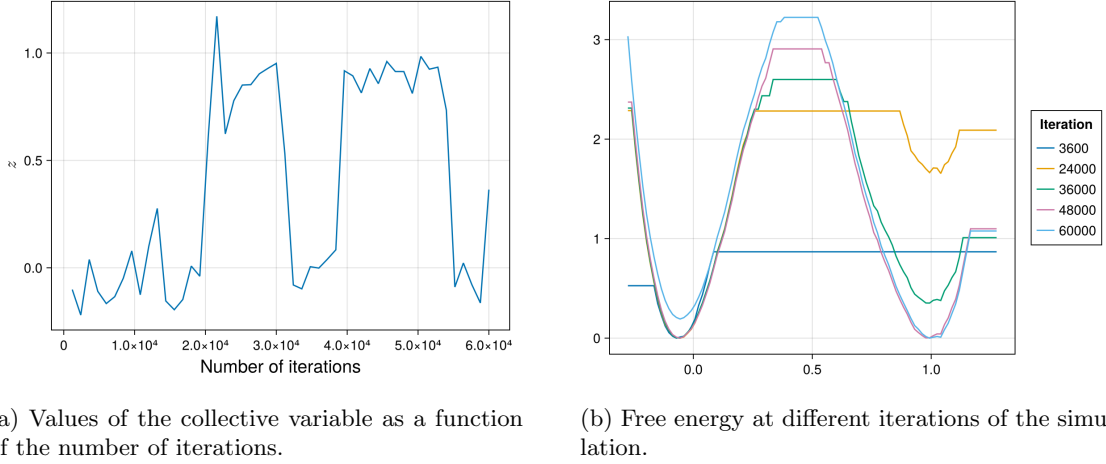
- $n = 3600$: no transition has happened yet, only the left well has been sampled sufficiently so that nonzero values for the free energy are observed;
- $n = 24,000$: one transition has happened, the right well is being sampled, balancing the values of the free energy between the two modes;
- $n = 36,000$: two transitions have happened, the free energy is almost converged;
- $n = 48,000$: three transitions have happened, the profile of the free energy is now similar to the one obtained to the reference profile obtained using thermodynamic integration, see Figure 1b;
- $n = 60,000$: four transitions have happened and one is being observed, the free energy profile do not change significantly.

3 Optimizing the diffusion: the kinetic case

First introduced in [12], HMC algorithms generates a Markov chain $(q^n, p^n)_{n \geq 0}$ in the augmented space $\mathcal{Q} \times \mathbb{R}^d$ such that the marginal in position of the equilibrium probability distribution is the target Gibbs probability distribution π defined in (2). The additional variable p^n is a momentum associated with the position q^n . HMC algorithms are built on three blocks: (i) a partial or full resampling of the momentum variable, (ii) the integration of Hamiltonian dynamics using the Generalized Störmer–Verlet (GSV) scheme [19] and (iii) a Metropolis–Hastings accept/reject procedure. When the momentum variable is partially refreshed, the algorithm is referred to as a Generalized HMC algorithm [21]. If the Hamiltonian function is denoted by H , then the density of the equilibrium probability distribution of the Markov chain is proportional to $e^{-\beta H}$, and H is constructed such that its marginal in position is exactly the Gibbs measure π defined by (2).

Standard HMC algorithms relies on the Hamiltonian function

$$H(q, p) = V(q) + \frac{1}{2} p^\top M^{-1} p, \quad (36)$$



(a) Values of the collective variable as a function of the number of iterations.

(b) Free energy at different iterations of the simulation.

Figure 4: Behavior of the free energy and the values of the collective variable during a sample trajectory using Algorithm 2.

where M is a positive definite symmetric matrix which can be tuned to precondition the Hamiltonian dynamics. It is easily checked, using the separability of the Hamiltonian function, that the marginal in position of the equilibrium distribution is π . The Hamiltonian dynamics is integrated using the Störmer–Verlet (SV), or *leapfrog*, numerical scheme: $(q^{n+1}, p^{n+1}) = \varphi_{\Delta t}^{\text{SV}}(q^n, p^n)$ where

$$\begin{cases} p^{n+1/2} = p^n - \frac{\Delta t}{2} \nabla V(q^n), \\ q^{n+1} = q^n + \Delta t M^{-1} p, \\ p^{n+1} = p^{n+1/2} - \frac{\Delta t}{2} \nabla V(q^{n+1}), \end{cases}$$

The flow $\varphi_{\Delta t}^{\text{SV}}$ is such that

$$S \circ \varphi_{\Delta t}^{\text{SV}} \circ S \circ \varphi_{\Delta t}^{\text{SV}} = \text{id}_{\mathcal{Q}}, \quad (37)$$

where S is the momentum reversal map: $S(q, p) = (q, -p)$. The property (37) is needed to ensure that the sampling is unbiased [19].

To introduce a nonconstant diffusion D , one can generalize the Hamiltonian function (36) by introducing

$$H(q, p) = V(q) - \frac{1}{2} \ln \det D(q) + \frac{1}{2} p^\top D(q) p. \quad (38)$$

This Hamiltonian function is the one considered in the Riemann Manifold HMC (RMHMC) algorithm which was introduced in [14]. It reduces to (36) when the diffusion is taken to be the identity matrix. One can check that the marginal in position of the equilibrium distribution is still the Gibbs measure π , whatever the diffusion matrix D . The RMHMC algorithm can be shown to yield a (weakly) consistent discretization of the overdamped Langevin dynamics (3), see [30, Section 3.3]. This motivates the link between the diffusion D in (38) and the diffusion D , seen as the inverse of a position-dependent mass matrix, in (3).

Since the Hamiltonian function (38) is not separable, one has to use the Generalized Störmer–Verlet (GSV) numerical scheme to integrate the dynamics. For a given configuration $(q^n, p^n) \in \mathcal{Q} \times \mathbb{R}^d$, this numerical scheme writes

$$\begin{cases} p^{n+1/2} = p^n - \frac{\Delta t}{2} \nabla_q H(q^n, p^{n+1/2}), \\ q^{n+1} = q^n + \frac{\Delta t}{2} \left(\nabla_p H(q^n, p^{n+1/2}) + \nabla_p H(q^{n+1}, p^{n+1/2}) \right), \\ p^{n+1} = p^{n+1/2} - \frac{\Delta t}{2} \nabla_q H(q^{n+1}, p^{n+1/2}). \end{cases} \quad (39)$$

Note that it reduces to the SV numerical scheme when setting the diffusion to the identity matrix. The notable change with the standard HMC algorithm is that the first two steps of GSV in (39) are implicit. In practice, they are thus solved using Newton’s method. As discussed in [30], this may introduce a bias, related to the fact that the implicit problem may have multiple or no solution, and the property (37) may not hold for the numerical flow implemented in practice. To remedy this issue, reversibility checks have been introduced, first to sample probability measures on submanifolds [43, 34, 32], then in the context of RMHMC [15, 36] and for general Hamiltonian functions [30]. Given a numerical flow $\varphi_{\Delta t}$ that attempts at integrating (39) (*e.g.* using Newton’s method), one defines a *numerical flow with reversibility checks* by

$$\forall (q, p) \in \mathcal{Q} \times \mathbb{R}^d, \quad \varphi_{\Delta t}^{\text{rev}}(q, p) = \varphi_{\Delta t}(q, p) \mathbb{1}_{(q,p) \in \mathcal{B}_{\Delta t}} + S(q, p) \mathbb{1}_{(q,p) \notin \mathcal{B}_{\Delta t}}, \quad (40)$$

where the set $\mathcal{B}_{\Delta t}$ is defined as the set of configurations $(q, p) \in \mathcal{Q} \times \mathbb{R}^d$ such that the property (37) holds, namely:

- the Newton method for the *forward* problem is converging so that $\varphi_{\Delta t}(q, p)$ is well-defined,
- the Newton method for the *backward* problem, namely starting from $(q, -p)$, is converging so that $\varphi_{\Delta t} \circ S \circ \varphi_{\Delta t}(q, p)$ is well-defined,
- the solutions to the forward and backward problems satisfy the reversibility property (37).

It is then easy to check that the property (37) holds for the flow with reversibility checks $\varphi_{\Delta t}^{\text{rev}}$. Moreover, one can check that $\varphi_{\Delta t}^{\text{rev}}$ is a measurable map which preserves the Lebesgue measure over \mathcal{Q} . These two ingredients ensure that the RM(G)HMC algorithms are unbiased. We refer to [30] for precise definitions and results.

For the diffusion (12), the Hamiltonian function (38) rewrites

$$H(q, p) = V(q) - \frac{d}{2} \ln \kappa_\alpha - \frac{1}{2} \ln a_\alpha(\xi(q)) + \frac{\kappa_\alpha}{2} p^\top p + \frac{\kappa_\alpha}{2} (a_\alpha(\xi(q)) - 1) \frac{(\nabla \xi(q) \cdot p)^2}{\|\nabla \xi(q)\|^2}. \quad (41)$$

The second term in (41) is constant and can be omitted.

Outline of the section. In Section 3.1, we describe the RM(G)HMC algorithms using the diffusion (12). In particular, we make precise the implementation of Newton’s method, and describe how the numerical reversibility checks are done in practice. We then present the numerical results in Section 3.2.

Note that we still name these algorithms RM(G)HMC even though they contain reversibility checks, which may not be a standard denomination in the literature.

3.1 Algorithms and reversibility checks

We make precise in Section 3.1.1 the RMHMC algorithm, and in particular how to integrate the Hamiltonian dynamics with Hamiltonian function (41) using Newton’s method. This will also highlight how the implementation can be simplified in the case when the collective variable is a function of only a few components of the position variable. We then describe in Section 3.1.2 the RMGHMC algorithm, which relies on the integration of an Ornstein–Uhlenbeck process to partially refresh the momenta.

3.1.1 RMHMC

The RMHMC algorithm with reversibility checks is detailed in Algorithm 3. Let us comment on the various steps of this algorithm. In Step [3.i], the momenta is fully resampled according to the marginal in momenta of the measure whose density is proportional to $e^{-\beta H}$. In view of (38), one easily sees that it is a Gaussian probability distribution with zero mean and covariance matrix $D(q)^{-1}$. In Step [3.ii], the Hamiltonian dynamics is integrated using the modified GSV

Algorithm 3 RMHMC algorithm with reversibility checks.

Consider an initial condition $(q^0, p^0) \in \mathcal{Q} \times \mathbb{R}^d$, and set $n = 0$.

[3.i] Sample $\tilde{p}^n \sim \mathcal{N}(0, D(q^n)^{-1})$;

[3.ii] Apply one step of the Hamiltonian dynamics with momentum reversal and S -reversibility check:

$$(\tilde{q}^{n+1}, \tilde{p}^{n+1}) = \varphi_{\Delta t}^{\text{rev}}(q^n, \tilde{p}^n),$$

where $\varphi_{\Delta t}^{\text{rev}}$ is defined by (40);

[3.iii] Draw a random variable U^n with uniform law on $[0, 1]$:

- if $U^n \leq \exp(\beta (H(q^n, \tilde{p}^n) - H(\tilde{q}^{n+1}, \tilde{p}^{n+1})))$, accept the proposal and set $(q^{n+1}, p^{n+1}) = (\tilde{q}^{n+1}, \tilde{p}^{n+1})$;
- else reject the proposal and set $(q^{n+1}, p^{n+1}) = (q^n, \tilde{p}^n)$;

[3.iv] Increment n and go back to [3.i].

flow with reversibility checks (40). We discuss below how this is done in practice using Newton's method. Lastly, Step [3.iii] is a Metropolis–Hastings accept/reject procedure. Note that the sign of the momentum variable is not relevant when accepting or rejecting a proposal as the momenta are fully resampled at each iteration.

Hamiltonian dynamics' integration in practice using Newton's method. Let us make precise how the Hamiltonian dynamics are integrated using the GSV scheme (39) and Newton's method. In particular, this will highlight how we can limit the computational overhead compared to the standard HMC algorithm when the collective variable is a function of a small number of components.

The gradients of the Hamiltonian function (41) are given by

$$\begin{aligned} \nabla_q H(q, p) &= \nabla V(q) - \frac{1}{2} \frac{a'_\alpha(\xi(q))}{a_\alpha(\xi(q))} \nabla \xi(q) + \frac{\kappa_\alpha}{2} \frac{(\nabla \xi(q) \cdot p)^2 a'_\alpha(\xi(q))}{\|\nabla \xi(q)\|^2} \nabla \xi(q) \\ &\quad + \kappa_\alpha (a_\alpha(\xi(q)) - 1) \frac{(\nabla \xi(q) \cdot p)}{\|\nabla \xi(q)\|^2} \nabla^2 \xi(q) p \\ &\quad - \kappa_\alpha (a_\alpha(\xi(q)) - 1) \frac{(\nabla \xi(q) \cdot p)^2}{\|\nabla \xi(q)\|^4} \nabla^2 \xi(q) \nabla \xi(q). \end{aligned} \quad (42)$$

and

$$\nabla_p H(q, p) = \kappa_\alpha p + \kappa_\alpha (a_\alpha(\xi(q)) - 1) \frac{\nabla \xi(q) \cdot p}{\|\nabla \xi(q)\|^2} \nabla \xi(q).$$

Solving the implicit problem on the momenta. Recall that the GSV scheme is defined in (39). To solve for $p^{n+1/2}$ we introduce the map $g(\cdot; q^n, p^n)$ defined by

$$\begin{aligned} g(p; q^n, p^n) &= p - p^n + \frac{\Delta t}{2} \nabla V(q^n) - \frac{\Delta t}{4} \frac{a'_\alpha(\xi(q^n))}{a_\alpha(\xi(q^n))} \nabla \xi(q^n) + \frac{\kappa_\alpha \Delta t}{4} \frac{(\nabla \xi(q^n) \cdot p)^2 a'_\alpha(\xi(q^n))}{\|\nabla \xi(q^n)\|^2} \nabla \xi(q^n) \\ &\quad + \frac{\kappa_\alpha \Delta t}{2} (a_\alpha(\xi(q^n)) - 1) \frac{(\nabla \xi(q^n) \cdot p)}{\|\nabla \xi(q^n)\|^2} \nabla^2 \xi(q^n) p \\ &\quad - \frac{\kappa_\alpha \Delta t}{2} (a_\alpha(\xi(q^n)) - 1) \frac{(\nabla \xi(q^n) \cdot p)^2}{\|\nabla \xi(q^n)\|^4} \nabla^2 \xi(q^n) \nabla \xi(q^n). \end{aligned} \quad (43)$$

We want to find $p^{n+1/2}$ that solves $g(p^{n+1/2}, q^n, p^n) = 0$. The Jacobian matrix of g at a point p is given by

$$\begin{aligned}\nabla g(p; q^n, p^n) &= \mathbf{I}_d + \frac{\kappa_\alpha \Delta t}{2} \frac{(\nabla \xi(q^n) \cdot p) a'_\alpha(\xi(q^n))}{\|\nabla \xi(q^n)\|^2} \nabla \xi(q^n) \otimes \nabla \xi(q^n) \\ &\quad + \frac{\kappa_\alpha \Delta t}{2} \frac{a_\alpha(\xi(q^n)) - 1}{\|\nabla \xi(q^n)\|^2} [\nabla^2 \xi(q^n) p] \otimes \nabla \xi(q^n) \\ &\quad + \frac{\kappa_\alpha \Delta t}{2} (a_\alpha(\xi(q^n)) - 1) \frac{\nabla \xi(q^n) \cdot p}{\|\nabla \xi(q^n)\|^2} \nabla^2 \xi(q^n) \\ &\quad - \kappa_\alpha \Delta t (a_\alpha(\xi(q^n)) - 1) \frac{\nabla \xi(q^n) \cdot p}{\|\nabla \xi(q^n)\|^4} [\nabla^2 \xi(q^n) \nabla \xi(q^n)] \otimes \nabla \xi(q^n)\end{aligned}\quad (44)$$

We then define the Newton sequence as follows: let $p^{n+1/2,0} = p^{n+1/2}$ and $p^{n+1/2,1} = p^n - \frac{\Delta t}{2} \nabla_q H(q^n, p^n)$, and for any $i \geq 1$,

$$p^{n+1/2,i+1} = p^{n+1/2,i} - \left(\nabla g(p^{n+1/2,i}, q^n, p^n) \right)^{-1} g(p^{n+1/2,i}, q^n, p^n).$$

In practice, the linear system

$$\nabla g(p^{n+1/2,i}, q^n, p^n) u = -g(p^{n+1/2,i}, q^n, p^n), \quad (45)$$

is solved for the unknown $u = p^{n+1/2,i+1} - p^{n+1/2,i}$. The Newton sequence is constructed iteratively, until a maximum number of iterations N_{Newton} has been attained or when stopping criteria of the following form are met:

$$\left\| p^{n+1/2,i+1} - p^{n+1/2,i} \right\| < \eta_{\text{Newton,Cauchy}}, \quad \left\| g(p^{n+1/2,i+1}) \right\| < \eta_{\text{Newton,root}}, \quad (46)$$

where $\eta_{\text{Newton,Cauchy}}, \eta_{\text{Newton,root}}$ are user-defined thresholds. When the maximum number of iterations is attained without obtaining convergence, or when the matrix ∇g is not (numerically) invertible, the computation fails and $S(q^n, p^n)$ is returned (see (40)).

Solving the implicit problem on the position. If the first implicit problem succeeded, one can proceed and try to compute the new position q^{n+1} . let us define to this end the map

$$\begin{aligned}h(q; q^n, p^{n+1/2}) &= q - q^n - \kappa_\alpha \Delta t p^{n+1/2} - \frac{\kappa_\alpha \Delta t}{2} (a_\alpha(\xi(q^n)) - 1) \frac{\nabla \xi(q^n) \cdot p^{n+1/2}}{\|\nabla \xi(q^n)\|^2} \nabla \xi(q^n) \\ &\quad - \frac{\kappa_\alpha \Delta t}{2} (a_\alpha(\xi(q)) - 1) \frac{\nabla \xi(q) \cdot p^{n+1/2}}{\|\nabla \xi(q)\|^2} \nabla \xi(q).\end{aligned}\quad (47)$$

We want to find q^{n+1} that solves $h(q^{n+1}, q^n, p^{n+1/2}) = 0$. The Jacobian of h at a point q is given by

$$\begin{aligned}\nabla h(q; q^n, p^{n+1/2}) &= \mathbf{I}_d - \frac{\kappa_\alpha \Delta t}{2} \frac{(\nabla \xi(q) \cdot p^{n+1/2}) a'_\alpha(\xi(q))}{\|\nabla \xi(q)\|^2} \nabla \xi(q) \otimes \nabla \xi(q) \\ &\quad - \frac{\kappa_\alpha \Delta t}{2} \frac{a_\alpha(\xi(q)) - 1}{\|\nabla \xi(q)\|^2} \nabla \xi(q) \otimes [\nabla^2 \xi(q) p^{n+1/2}] \\ &\quad + \kappa_\alpha \Delta t (a_\alpha(\xi(q)) - 1) \frac{\nabla \xi(q) \cdot p^{n+1/2}}{\|\nabla \xi(q)\|^4} [\nabla^2 \xi(q) \nabla \xi(q)] \otimes \nabla \xi(q) \\ &\quad - \frac{\kappa_\alpha \Delta t}{2} (a_\alpha(\xi(q)) - 1) \frac{\nabla \xi(q) \cdot p^{n+1/2}}{\|\nabla \xi(q)\|^2} \nabla^2 \xi(q).\end{aligned}\quad (48)$$

We then follow a similar strategy as for the first implicit problem. If the computations fail, the flow again returns $S(q^n, p^n)$. We emphasize that the forces $-\nabla V$ need to be computed only once per integration of the Hamiltonian dynamics.

Remark 3. When $\|\nabla\xi\|$ is constant, any term of the form $\nabla^2\xi(q)\nabla\xi(q)$ appearing in (42), (43), (44), (48) vanishes.

Numerical reversibility check. If all the Newton’s method needed to defined $\varphi_{\Delta t}\circ S\circ\varphi_{\Delta t}(q,p)$ have converged, then the reversibility check (37) is performed. In practice, it is done using a user defined threshold η_{rev} , and stating that the property (37) *numerically* holds when

$$\|S\circ\varphi_{\Delta t}\circ S\circ\varphi_{\Delta t}(q,p)-(q,p)\|<\eta_{\text{rev}}. \quad (49)$$

Optimization of the implementation of RMHMC. In view of the various formulas needed to run Newton’s method, the additional computations (compared to the standard HMC scheme) only require gradients or Hessians of the collective variable. When the collective variable is a function of only a few components of the position q , one can therefore limit computational overheads and the associated storage capacity, as already discussed for MALA in Section 2.3. As a guiding example, consider the physical system used for our numerical experiment in Section 2.3. The gradient of ξ only contains 4 nonzero components (see (31)) and the Hessian of ξ only contains a 4×4 nonzero submatrix, so that only the first four components in (43)-(47) are notably modified (compared to the standard HMC scheme). Furthermore, the matrices ∇g and ∇h appearing in (44)-(48) are block diagonal with a structure similar to the diffusion, see (32). This means that the update of the Newton sequence described in (45) can be done by (i) solving only a 4×4 linear system for the first 4 components and (ii) updating the other components as the update is explicit for these components. These observations can be generalized to any collective variable which is a function of only $k\leq d$ components of the positions.

3.1.2 RMGHMC

This section is based on [30, Section 3.2.1]. The GHMC algorithm is related to a discretization of the Langevin dynamics, which writes

$$\begin{cases} dq_t = D(q_t)p_t dt, \\ dp_t = -\nabla_q H(q_t, p_t) dt - \gamma D(q_t)p_t dt + \sqrt{\frac{2\gamma}{\beta}} dW_t, \end{cases} \quad (50)$$

where $\gamma > 0$ is a friction parameter, and $(W_t)_{t\geq 0}$ is a standard d -dimensional Brownian motion. The GHMC algorithm is built using a splitting technique, considering separately the Hamiltonian and fluctuation-dissipation parts of the dynamics. Here, the fluctuation-dissipation part of the dynamics is simply an Ornstein–Uhlenbeck process, inducing a partial refreshment of the momenta instead of a full resampling as in the RMHMC algorithm 3. To integrate the Ornstein–Uhlenbeck process for a fixed position q^n , namely

$$dp_t = -\gamma D(q^n)p_t dt + \sqrt{\frac{2\gamma}{\beta}} dW_t, \quad (51)$$

we use a midpoint Euler scheme: using a time increment $\Delta t/2$, this scheme reads

$$p^{n+1/4} = p^n - \frac{\Delta t}{4}\gamma D(q^n)(p^n + p^{n+1/4}) + \sqrt{\gamma\beta^{-1}\Delta t} G^n.$$

This requires solving the linear system

$$\left[\mathbf{I}_d + \frac{\Delta t}{4}\gamma D(q^n)\right] p^{n+1/4} = \left[\mathbf{I}_d - \frac{\Delta t}{4}\gamma D(q^n)\right] p^n + \sqrt{\gamma\beta^{-1}\Delta t} G^n,$$

which has a unique solution:

$$p^{n+1/4} = \left[\mathbf{I}_d + \frac{\Delta t}{4}\gamma D(q^n)\right]^{-1} \left[\left(\mathbf{I}_d - \frac{\Delta t}{4}\gamma D(q^n)\right) p^n + \sqrt{\gamma\beta^{-1}\Delta t} G^n\right]. \quad (52)$$

This defines the map $\varphi_{\Delta t/2}^{\text{OU}}$:

$$\varphi_{\Delta t/2}^{\text{OU}}(q^n, p^n, G^n) = (q^n, p^{n+1/4}).$$

A Strang splitting based on these elements leads to Algorithm 4. The main difference with Algorithm 3 is that the momenta are not discarded, but partially refreshed at Steps [4.i] and [4.v]. Notice that the momenta has its sign reversed at Step [4.iv]: this is only needed for consistency of the RMGHMC algorithm with the Langevin dynamics. The sign of the momenta is changed only if rejection happens either in Step [4.ii] or in Step [4.iii].

Algorithm 4 RMGHMC algorithm with reversibility checks.

Consider an initial condition $(q^0, p^0) \in \mathcal{Q} \times \mathbb{R}^d$, and set $n = 0$.

[4.i] Evolve the momenta by integrating the fluctuation-dissipation part with time increment $\Delta t/2$: $(q^n, p^{n+1/4}) = \varphi_{\Delta t/2}^{\text{OU}}(q^n, p^n, G^n)$.

[4.ii] Apply one step of the Hamiltonian dynamics with momentum reversal and S -reversibility check:

$$(\tilde{q}^{n+1}, \tilde{p}^{n+3/4}) = S \circ \varphi_{\Delta t}^{\text{rev}}(q^n, p^{n+1/4}),$$

where $\varphi_{\Delta t}^{\text{rev}}$ is defined in (40);

[4.iii] Draw a random variable U^n with uniform law on $(0, 1)$:

- if $U^n \leq \exp(-H(\tilde{q}^{n+1}, \tilde{p}^{n+3/4}) + H(q^n, p^{n+1/4}))$, accept the proposal and set $(q^{n+1}, p^{n+3/4}) = (\tilde{q}^{n+1}, \tilde{p}^{n+3/4})$;
- else reject the proposal and set $(q^{n+1}, p^{n+3/4}) = (q^n, p^{n+1/4})$.

[4.iv] Reverse the momenta as $\tilde{p}^{n+1} = -p^{n+3/4}$.

[4.v] Evolve the momenta by integrating the fluctuation-dissipation part with time increment $\Delta t/2$: $(q^{n+1}, p^{n+1}) = \varphi_{\Delta t/2}^{\text{OU}}(q^{n+1}, \tilde{p}^{n+1}, G^{n+1/2})$.

[4.vi] Increment n and go back to [4.i].

Remark 4. Note that for the diffusion (12), the update (52) can be performed without solving a linear system, as the matrix

$$\mathbf{I}_d + \frac{\Delta t}{4} \gamma D_\alpha(q^n) = \left(1 + \frac{\Delta t}{4} \gamma \kappa_\alpha\right) P^\perp(q^n) + \left(1 + \frac{\Delta t}{4} \gamma \kappa_\alpha a \circ \xi(q^n)\right) P(q^n),$$

has an explicit inverse:

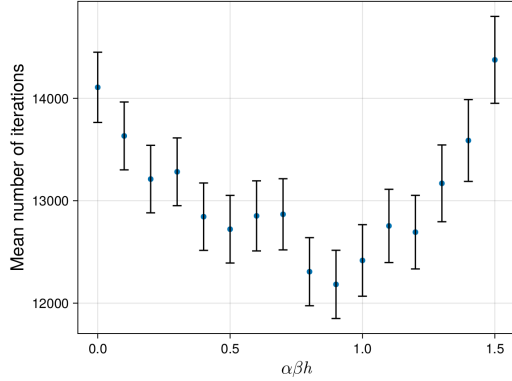
$$\left(1 + \frac{\Delta t}{4} \gamma \kappa_\alpha\right)^{-1} P^\perp(q^n) + \left(1 + \frac{\Delta t}{4} \gamma \kappa_\alpha a \circ \xi(q^n)\right)^{-1} P(q^n).$$

3.2 Numerical results

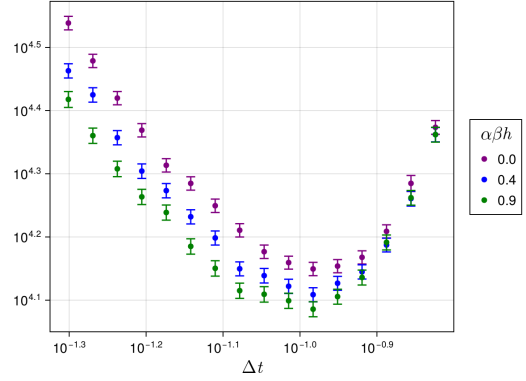
The numerical experiment is the same as in Section 2.3. The values of $\alpha\beta h$ presented in the results, as well as the time interval the optimal time step is searched on, are scheme dependent: we choose 16 values of the time step evenly spaced log-wise on the interval $[\Delta t_{\min}, \Delta t_{\max}]$ with

- for RMHMC: $\Delta t_{\min} = 5 \times 10^{-2}$, $\Delta t_{\max} = 1.5 \times 10^{-1}$ and $\alpha\beta h \in \{0, 0.1, \dots, 1.5\}$;
- for RMGHMC: $\Delta t_{\min} = 10^{-2}$ and $\Delta t_{\max} = 10^{-1}$ and $\alpha\beta h \in \{0, 0.1, \dots, 2.4\}$.

In each case, results for larger values of $\alpha\beta h$ worsen: transition times increase up to the point when the dynamics become unstable.

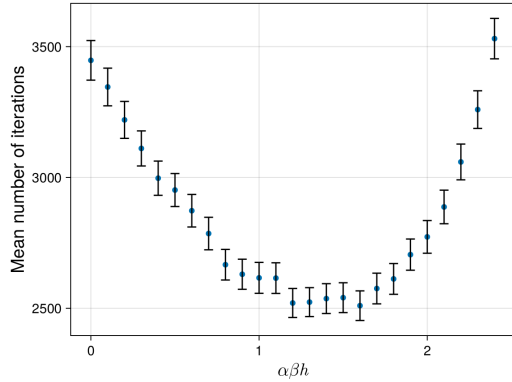


(a) Minimum values over the range of time steps for each value of α .

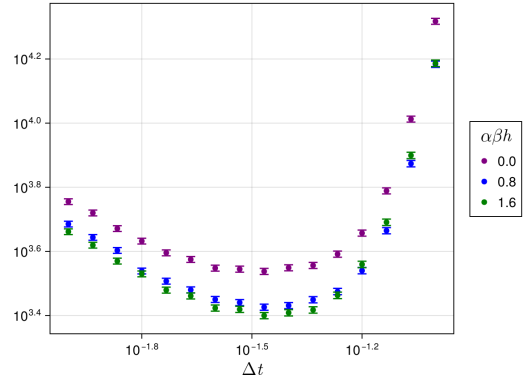


(b) Mean number of iterations as a function of Δt for some values of α .

Figure 5: Sampling efficiency using the RMHMC algorithm 3.



(a) Minimum values over the range of time steps for each value of α .



(b) Mean number of iterations as a function of Δt for some values of α .

Figure 6: Sampling efficiency using the RMGHMC algorithm 4.

Hyperparameters. The maximum number of iterations for Newton’s method is set to $N_{\text{Newton}} = 100$, and we use $\eta_{\text{Newton,Cauchy}} = \eta_{\text{Newton,root}} = 10^{-12}$ for the tolerance checks in Newton’s method, see (46). The tolerance for the reversibility check is set to $\eta_{\text{rev}} = 10^{-6}$, see (49). Note that in our case, we set the tolerance for the reversibility check in (49) smaller than the tolerances for Newton’s method in (46) in order to take into account the accumulating round-off errors when checking for numerical reversibility. We checked that, in our numerical experiment, when (49) does not hold, the value of the left-hand side is orders of magnitude larger than the tolerance used.

For the RMGHMC algorithm, we set $\gamma = 1$. This hyperparameter could be made position-dependent and be optimized as well, as was done for instance in [6], this is left for future works. The uninformed choice $\gamma = 1$ is motivated by hypocoercivity results on weighted L^2 spaces for the Langevin dynamics, as the rate of convergence towards equilibrium is lower bounded by $\min(\gamma, \gamma^{-1})$ (up to a multiplicative constant), see for instance [11, 16]. The choice $\gamma = 1$ therefore provides a balance between the limit $\gamma \rightarrow 0$, where the Langevin dynamics reduces to the Hamiltonian dynamics, and $\gamma \rightarrow +\infty$, where the Langevin dynamics converge to the over-damped Langevin dynamics (3) [22, 42].

Mean number of iterations in-between transitions. The results using the RMHMC (respectively the RMGHMC) algorithm are presented in Figure 5 (respectively in Figure 6). For RMHMC, we obtain $\widehat{\tau}(\alpha_{\text{opt}})^* = 12183$ for $\alpha_{\text{opt}} = 0.45$, while $\widehat{\tau}(0)^* = 14107$. For RMGHMC, we obtain $\widehat{\tau}(\alpha_{\text{opt}})^* = 2510$ for $\alpha_{\text{opt}} = 0.8$, while $\widehat{\tau}(0)^* = 3448$. The results for RMHMC are comparable to what has been obtained for MALA in Sections 2.3 and 2.5, maybe a bit worse because of rejections due to the implicit problems (see the paragraph below). However, the results for RMGHMC are significantly better, which shows the relevance of building samplers in the phase space and performing the very modest computational overheads related to the Ornstein–Uhlenbeck dynamics (51). For both algorithms, we observe a great reduction in the mean number of iterations when choosing multiplicative noise (*i.e.* a positive value of α) instead of additive noise (*i.e.* $\alpha = 0$). In practice, values of α such that the argument of the exponential in (12) is overall close to 1 is observed to be a good rule of thumb in order to choose the relevant value of the hyperparameter α .

Note that the mean number of iterations scales in the limit $\Delta t \rightarrow 0$ as Δt^{-1} for the RMGHMC algorithm while it scales as Δt^{-2} for the RMHMC algorithm. This is consistent with the fact that

- RMGHMC formally yields a consistent discretization of the Langevin dynamics (50) (see [30, Section 3.2.2]), so that $t_{\text{sim}} = N_{\text{iter}}\Delta t$;
- RMHMC yields a weakly consistent discretization of the overdamped Langevin dynamics (3) with effective time step $h = \Delta t^2/2$ (see [30, Section 3.3]), so that $t_{\text{sim}} = N_{\text{iter}}h$.

Even though the optimal time steps may not correspond to the limiting regime $\Delta t \rightarrow 0$, we still observe that the optimal time step for the RMHMC algorithm $\Delta t_{\text{RMHMC}}^*$ is related to the optimal time step for the RMGHMC algorithm $\Delta t_{\text{RMGHMC}}^*$ as $\Delta t_{\text{RMHMC}}^* \approx \sqrt{\Delta t_{\text{RMGHMC}}^*}$. This explains why, in order to obtain an optimal time step with respect to the mean number of iterations in-between transitions, the interval of values for RMHMC contain larger values than for RMGHMC. Lastly, this means that, for small time steps, the extra computations performed by integrating the Ornstein–Uhlenbeck process (51) are negligible compared to running the RMHMC algorithm (since the number of iterations greatly increases for the latter algorithm).

Rejection probabilities. When the time step Δt becomes large, it is expected that rejections because of nonconvergence when solving the implicit problems increase. To have an idea of how much these rejections impact the computational costs, we present in Figure 7 the various rejection probabilities when using the RMHMC algorithms with $\alpha\beta h = 2.0$. For each value of Δt , we run the RMHMC algorithm 10^6 times starting from q^0 defined in (33) (*i.e.* we perform one step, and then fix the position to q^0 again). We then count how many rejections were due to

- not being able to solve for $p^{n+1/2}$ in (39) in the *forward* pass (labeled ‘Forward (momenta)’);
- having succeeded, not being able to solve for q^{n+1} in (39) in the *forward* pass (labeled ‘Forward (position)’);
- having succeeded, not being able to solve for $p^{n+1/2}$ in (39) in the *backward* pass (labeled ‘Backward (momenta)’);
- having succeeded, not being able to solve for q^{n+1} in (39) in the *backward* pass (labeled ‘Backward (position)’);
- having succeeded, not observing numerical reversibility (49) (labeled ‘Reversibility’);
- having succeeded, the Metropolis–Hastings accept/reject procedure (labeled ‘Metropolis–Hastings’).

We then divide each number by the number of tries to obtain ratios, which are then transformed into percentages. Let us emphasize that the rejection procedures are performed sequentially, as stated above. Figure 7b presents the results for the interval of time steps used in the numerical

$\alpha\beta h$	Δt	Forward		Backward		Reversibility	Metropolis–Hastings	Global
		Momenta	Position	Momenta	Position			
0.0	1.0×10^{-1}	0.0	0.0	0.0	0.0	0.0	8.5×10^{-2}	8.5×10^{-2}
0.5	9.7×10^{-2}	0.0	6.6×10^{-3}	0.0	0.0	0.0	1.6×10^{-1}	1.6×10^{-1}
0.9	1.0×10^{-1}	0.0	1.9×10^{-1}	0.0	1.3×10^{-1}	2.7×10^{-2}	5.6×10^{-1}	9.0×10^{-1}
1.5	9.0×10^{-2}	0.0	3.3×10^{-1}	4.0×10^{-4}	6.0×10^{-1}	1.6	1.3×10^{-1}	2.6
2.0	8.3×10^{-2}	0.0	1.6	1.5×10^{-2}	3.9×10^{-3}	2.2	2.0×10^{-1}	4.1

Table 1: Decomposition in percentages of the rejection probabilities for various values of α and their corresponding optimal time step Δt . “Forward” refers to non-convergent iterations to solve the implicit forward problem; “Backward” refers to a convergence of the implicit forward problem but a non-convergent implicit backward problem; “Reversibility” refers to convergent implicit forward and backward problems for which (37) is not satisfied; upon acceptance in the three previous steps, “Metropolis–Hastings” refers to a rejection in the acceptance/rejection of Step [3.iii] in the RMHMC algorithm. Finally, “Global” is the global rejection probability, namely the sum of all the previous columns.

experiment, while Figure 7a shows the rejection probabilities for a larger interval of values of the time step. The latter figure is to show that the rejections due to checking numerical reversibility eventually vanish when the time step becomes small, and that only rejections because of the Metropolis–Hastings accept/reject procedure are present. Looking at Figure 7b, we observe that rejections because of non-reversibility are present whatever the time step used. This shows the relevance of using reversibility checks in order to perform an unbiased sampling.

Notice that the rejection probability due to not being able to solve the *forward* implicit problem over the momenta is orders of magnitude smaller than the one due to the *forward* implicit problem over the position. This is because the equation for $p^{n+1/2}$ in (39) is actually quadratic in $p^{n+1/2}$, which is an easier problem to solve.

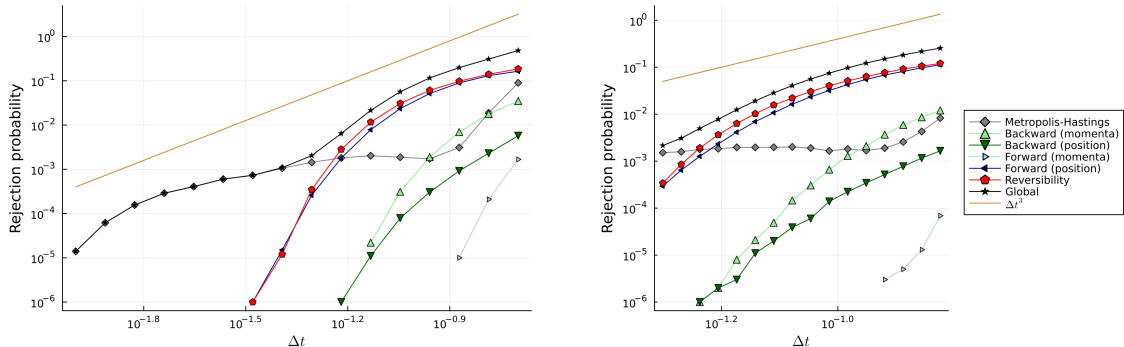
We give in Table 1 the decomposition of the rejection probabilities for various values of α and associated optimal time step. We observe a clear trend as α increases: the global rejection probability increases. As stated above, the implicit solve over momenta in the *forward* integration is observed to be successful. The main sources of rejections come from not reaching convergence for the implicit problem over the positions for the *forward* integration, and from not observing numerical reversibility. It may be surprising that the rejection probabilities due to not reaching convergence for the *backward* integration increases and then decreases. This is however expected since the rejection probability because of not solving the implicit problem over the position in the *forward* integration greatly increases, which lowers the number of proposals reaching the backward step. A similar situation is encountered for the Metropolis–Hastings rejection probability, as the rejection due to nonreversibility also greatly increases.

As for the RMGHMC scheme, we observed that rejections because of numerical nonreversibility for the various values of $\alpha\beta h$ only appeared for the largest value of the time step in the interval used for the numerical experiments, this is why we do not present the rejection probabilities for this scheme.

Of course, the results presented here depend on the implementation of the GSV solver (and to an extent to the way the Ornstein–Uhlenbeck is solved), and in particular in the choice of the hyperparameters $\eta_{\text{Newton,Cauchy}}, \eta_{\text{Newton,root}}, \eta_{\text{rev}}, N_{\text{Newton}}$. We checked that the values of the hyperparameters are reasonable, in the sense that lowering the tolerances or increasing the maximum number of iterations did not change the results significantly.

4 Perspectives

We introduced a class of diffusion matrices (12) that modifies the effective diffusion of overdamped Langevin dynamics in order for the effective dynamics to be governed by an effective diffusion coefficient leading to the fastest convergence in the homogenized regime (5). We provided a



(a) Rejection probabilities for 16 values of Δt evenly spaced log-wise in $[10^{-2}, 2 \times 10^{-1}]$

(b) Rejection probabilities for 16 values of Δt evenly spaced log-wise in $[5 \times 10^{-2}, 1.5 \times 10^{-1}]$

Figure 7: Rejection probabilities for $\alpha\beta h = 2.0$ for the RMHMC algorithm.

complete description of the methodology for one-dimensional collective variables. We list below a few perspectives that this work opens:

- The methodology developed in this work can be adapted to multidimensional collective variables upon finding a rationale for choosing the function a , which, in principle, is matrix-valued;
- For one-dimensional collective variables, there may be an interest in introducing an additional multiplicative parameter in a_α in order to balance the relative contributions of the projectors P and P^\perp in the definition of (12), see Remark 1;
- Other hyperparameters, such as the friction parameter γ in the RMGHMC algorithm, could be optimized to enhance convergence towards equilibrium;
- Another possible extension would be to directly optimize the diffusion in the latent space instead of relying on some parametric ansatz such as (12), utilizing the methodology developed in [9, 33]. As the latent space is usually one or two-dimensional, Finite Element methods could be used in order to directly optimize the effective diffusion by maximizing the spectral gap of the operator (with adjoints taken on $L^2(\xi \star \pi)$)

$$\mathcal{L}_{\sigma_a^2} = -\beta^{-1} \partial_z^* \sigma_a^2 \partial_z,$$

with respect to the map a , where σ_a is defined in (20);

- Lastly, since the mean force and free energy are learned in order to build the diffusion (12), one could use it in ABF methods in order to bias the dynamics, leading (once the estimated free energy is converged) to overdamped Langevin dynamics of the form

$$dq_t = (-D_\alpha(q_t) \nabla (V(q_t) - vF(\xi(q_t))) + \beta^{-1} \operatorname{div} D_\alpha(q_t)) dt + \sqrt{2\beta^{-1} D_\alpha(q_t)}^{1/2} dW_t,$$

with v a positive scaling parameter. Of course, this idea can also be applied to the Langevin dynamics as presented in Section 3. It would be interesting to understand how much can be gained in practice by blending these two ideas: free energy biasing, and introducing a positive dependent diffusion.

References

- [1] H. Alrachid and T. Lelièvre. Long-time convergence of an adaptive biasing force method: Variance reduction by Helmholtz projection. *SMAI J. Comput. Math.*, 1:55–82, 2015.

- [2] D. Bakry, I. Gentil, and M. Ledoux. *Analysis and Geometry of Markov Diffusion Operators*. Grundlehren der mathematischen Wissenschaften, Vol. 348. Springer, 2014.
- [3] A. Beskos, F. Pinski, J. Sanz-Serna, and A. Stuart. Hybrid Monte Carlo on Hilbert spaces. *Stochastic Processes and their Applications*, 121(10):2201–2230, 2011.
- [4] N. Bou-Rabee and A. Eberle. Two-scale coupling for preconditioned Hamiltonian Monte Carlo in infinite dimensions. *Stoch. Partial Differ. Equ. Anal. Comput.*, 9(1):207–242, 2021.
- [5] N. Bou-Rabee and J. M. Sanz-Serna. Geometric integrators and the Hamiltonian Monte Carlo method. *Acta Numerica*, 27:113–206, 2018.
- [6] M. Chak, N. Kantas, T. Lelièvre, and G. Pavliotis. Optimal friction matrix for underdamped langevin sampling. *ESAIM: Mathematical Modelling and Numerical Analysis*, 57(6):3335–3371, 2023.
- [7] C. Chipot and T. Lelièvre. Enhanced sampling of multidimensional free-energy landscapes using adaptive biasing forces. *SIAM J. Appl. Math.*, 71(5):1673–1695, 2011.
- [8] J. Comer, J. C. Gumbart, J. Hénin, T. Lelièvre, A. Pohorille, and C. Chipot. The Adaptive Biasing Force method: Everything you always wanted to know but were afraid to ask. *The Journal of Physical Chemistry B*, 119(3):1129–1151, 2015.
- [9] T. Cui, X. Tong, and O. Zahm. Optimal Riemannian metric for Poincaré inequalities and how to ideally precondition Langevin dynamics. *arXiv preprint*, 2404.02554, 2024.
- [10] E. Darve and A. Pohorille. Calculating free energies using average force. *The Journal of Chemical Physics*, 115(20):9169–9183, 2001.
- [11] J. Dolbeault, A. Klar, C. Mouhot, and C. Schmeiser. Exponential Rate of Convergence to Equilibrium for a Model Describing Fiber Lay-Down Processes. *Applied Mathematics Research eXpress*, 2013(2):165–175, 2012.
- [12] S. Duane, A. D. Kennedy, B. J. Pendleton, and D. Roweth. Hybrid Monte Carlo. *Physics Letters B*, 195(2):216–222, 1987.
- [13] V. Ehrlacher, T. Lelièvre, and P. Monmarché. Adaptive force biasing algorithms: New convergence results and tensor approximations of the bias. *The Annals of Applied Probability*, 32(5):3850 – 3888, 2022.
- [14] M. Girolami and B. Calderhead. Riemann Manifold Langevin and Hamiltonian Monte Carlo methods. *Journal of the Royal Statistical Society: Series B (Statistical Methodology)*, 73(2):123–214, 2011.
- [15] M. M. Graham, A. H. Thiery, and A. Beskos. Manifold Markov chain Monte Carlo methods for Bayesian inference in diffusion models. *Journal of the Royal Statistical Society Series B: Statistical Methodology*, 84(4):1229–1256, 2022.
- [16] M. Grothaus and P. Stilgenbauer. Hilbert space hypocoercivity for the Langevin dynamics revisited. *Methods Funct. Anal. Topology*, 22(2):152–168, 2016.
- [17] H. Haario, E. Saksman, and J. Tamminen. Adaptive proposal distribution for Random Walk Metropolis algorithm. *Computational Statistics*, 14(3):375–395, 1999.
- [18] H. Haario, E. Saksman, and J. Tamminen. An adaptive Metropolis algorithm. *Bernoulli*, 7(2):223–242, 2001.
- [19] E. Hairer, C. Lubich, and G. Wanner. *Geometric Numerical Integration*, volume 31 of *Springer Series in Computational Mathematics*. Springer-Verlag, Berlin, second edition, 2006.

- [20] W. K. Hastings. Monte Carlo sampling methods using Markov chains and their applications. *Biometrika*, 57(1):97–109, 1970.
- [21] A. M. Horowitz. A generalized guided Monte Carlo algorithm. *Physics Letters B*, 268(2):247–252, 1991.
- [22] S. Hottovy, A. McDaniel, G. Volpe, and J. Wehr. The Smoluchowski-Kramers limit of stochastic differential equations with arbitrary state-dependent friction. *Communications in Mathematical Physics*, 336(3):1259–1283, 2015.
- [23] J. Hénin and C. Chipot. Overcoming free energy barriers using unconstrained molecular dynamics simulations. *The Journal of Chemical Physics*, 121(7):2904–2914, 2004.
- [24] J. G. Kirkwood. Statistical mechanics of fluid mixtures. *The Journal of Chemical Physics*, 3(5):300–313, 1935.
- [25] F. Legoll and T. Lelièvre. Effective dynamics using conditional expectations. *Nonlinearity*, 23(9):2131, 2010.
- [26] T. Lelièvre and K. Minoukadeh. Long-time convergence of an adaptive biasing force method: the bi-channel case. *Arch. Ration. Mech. Anal.*, 202(1):1–34, 2011.
- [27] T. Lelièvre, F. Nier, and G. A. Pavliotis. Optimal non-reversible linear drift for the convergence to equilibrium of a diffusion. *Journal of Statistical Physics*, 152(2):237–274, 2013.
- [28] T. Lelièvre, M. Rousset, and G. Stoltz. Long-time convergence of an adaptive biasing force method. *Nonlinearity*, 21(6):1155–1181, 2008.
- [29] T. Lelièvre, M. Rousset, and G. Stoltz. *Free Energy Computations: A Mathematical Perspective*. Imperial College Press, 2010.
- [30] T. Lelièvre, R. Santet, and G. Stoltz. Unbiasing Hamiltonian Monte Carlo algorithms for a general hamiltonian function. *Foundations of Computational Mathematics*, 2024.
- [31] T. Lelièvre and G. Stoltz. Partial differential equations and stochastic methods in molecular dynamics. *Acta Numer.*, 25:681–880, 2016.
- [32] T. Lelièvre, G. Stoltz, and W. Zhang. Multiple projection Markov chain Monte Carlo algorithms on submanifolds. *IMA J. Numer. Anal.*, 43(2):737–788, 2023.
- [33] T. Lelièvre, G. A. Pavliotis, G. Robin, R. Santet, and G. Stoltz. Optimizing the diffusion coefficient of overdamped Langevin dynamics. *arXiv preprint*, 2404.12087, 2024.
- [34] T. Lelièvre, M. Rousset, and G. Stoltz. Hybrid Monte Carlo methods for sampling probability measures on submanifolds. *Numerische Mathematik*, 143(2):379–421, 2019.
- [35] N. Metropolis, A. W. Rosenbluth, M. N. Rosenbluth, A. H. Teller, and E. Teller. Equation of state calculations by fast computing machines. *The Journal of Chemical Physics*, 21(6):1087–1092, 1953.
- [36] M. Noble, V. D. Bortoli, and A. Durmus. Unbiased constrained sampling with self-concordant barrier Hamiltonian Monte Carlo. In *Thirty-seventh Conference on Neural Information Processing Systems*, 2023.
- [37] G. O. Roberts and J. S. Rosenthal. Coupling and ergodicity of adaptive Markov chain Monte Carlo algorithms. *J. Appl. Probab.*, 44(2):458–475, 2007.
- [38] G. O. Roberts and J. S. Rosenthal. Examples of adaptive MCMC. *J. Comput. Graph. Statist.*, 18(2):349–367, 2009.

- [39] G. O. Roberts and O. Stramer. Langevin diffusions and Metropolis-Hastings algorithms. *Methodol. Comput. Appl. Probab.*, 4:337–357 (2003), 2002.
- [40] G. O. Roberts and R. L. Tweedie. Exponential convergence of Langevin distributions and their discrete approximations. *Bernoulli*, 2(4):341–363, 1996.
- [41] P. J. Rossky, J. D. Doll, and H. L. Friedman. Brownian dynamics as smart Monte Carlo simulation. *J. Chem. Phys.*, 69(10):4628–4633, 1978.
- [42] M. Wang, D. Su, and W. Wang. Averaging on macroscopic scales with application to Smoluchowski–Kramers approximation. *Journal of Statistical Physics*, 191(2):22, 2024.
- [43] E. Zappa, M. Holmes-Cerfon, and J. Goodman. Monte Carlo on manifolds: Sampling densities and integrating functions. *Communications on Pure and Applied Mathematics*, 71(12):2609–2647, 2018.
- [44] W. Zhang, C. Hartmann, and C. Schütte. Effective dynamics along given reaction coordinates, and reaction rate theory. *Faraday Discuss.*, 195:365–394, 2016.

5 Proof of Proposition 1

We show that

$$b(z) = -\sigma^2(z)F'(z) + \beta^{-1}(\sigma^2)'(z).$$

To this end, we use the following lemma (see for instance [29, Lemma 3.10] or [25, Lemma 2.2]).

Lemma 1. *For any smooth function $\chi : \mathcal{Q} \rightarrow \mathbb{R}$, consider*

$$\chi^\xi(z) = \int_{\Sigma(z)} \chi \|\nabla \xi\|^{-1} d\sigma_{\Sigma(z)}.$$

The derivative of χ^ξ reads:

$$\frac{d\chi^\xi}{dz}(z) = \int_{\Sigma(z)} \left(\frac{\nabla \xi \cdot \nabla \chi}{\|\nabla \xi\|^2} + \chi \operatorname{div} \left(\frac{\nabla \xi}{\|\nabla \xi\|^2} \right) \right) \|\nabla \xi\|^{-1} d\sigma_{\Sigma(z)}.$$

In view of (6) and (7), it holds

$$d\pi^\xi = \frac{Z^{-1} e^{-\beta V} \|\nabla \xi\|^{-1} d\sigma_{\Sigma(z)}}{e^{-\beta F}},$$

so that, for instance,

$$\sigma^2(z) = \frac{Z^{-1} \int_{\Sigma(z)} \|\nabla \xi\|^2 e^{-\beta V} \|\nabla \xi\|^{-1} d\sigma_{\Sigma(z)}}{e^{-\beta F(z)}}.$$

It follows from Lemma 1 with $\chi = \|\nabla\xi\|^2 e^{-\beta V}$, that

$$\begin{aligned}
(\sigma^2)'(z) &= \frac{Z^{-1} \int_{\Sigma(z)} \left(\frac{\nabla\xi \cdot \nabla (\|\nabla\xi\|^2 e^{-\beta V})}{\|\nabla\xi\|^2} + \|\nabla\xi\|^2 e^{-\beta V} \operatorname{div} \left(\frac{\nabla\xi}{\|\nabla\xi\|^2} \right) \right) \|\nabla\xi\|^{-1} d\sigma_{\Sigma(z)}}{e^{-\beta F(z)}} \\
&\quad + \beta F'(z) \frac{Z^{-1} \int_{\Sigma(z)} \|\nabla\xi\|^2 e^{-\beta V} \|\nabla\xi\|^{-1} d\sigma_{\Sigma(z)}}{e^{-\beta F(z)}} \\
&= \frac{\int_{\Sigma(z)} \left(\frac{\nabla\xi \cdot \nabla (\|\nabla\xi\|^2)}{\|\nabla\xi\|^2} - \beta \nabla V \cdot \nabla\xi \right) Z^{-1} e^{-\beta V} \|\nabla\xi\|^{-1} d\sigma_{\Sigma(z)}}{e^{-\beta F(z)}} \\
&\quad + \frac{\int_{\Sigma(z)} \left(\Delta\xi + \|\nabla\xi\|^2 \frac{(-\nabla\xi \cdot \nabla (\|\nabla\xi\|^2))}{\|\nabla\xi\|^4} \right) Z^{-1} e^{-\beta V} \|\nabla\xi\|^{-1} d\sigma_{\Sigma(z)}}{e^{-\beta F(z)}} \\
&\quad + \beta F'(z) \sigma^2(z) \\
&= \beta \frac{\int_{\Sigma(z)} (-\nabla V \cdot \nabla\xi + \beta^{-1} \Delta\xi) Z^{-1} e^{-\beta V} \|\nabla\xi\|^{-1} d\sigma_{\Sigma(z)}}{e^{-\beta F(z)}} + \beta F'(z) \sigma^2(z) \\
&= \beta b(z) + \beta F'(z) \sigma^2(z).
\end{aligned}$$

This concludes the proof of the identity (16).

6 Proof of Proposition 2

The derivation of the effective dynamics for general diffusion processes (and for multivalued collective variables) is done in [44, Section 3.2]. Let us make precise the computations in the specific case of the dynamics (3) with diffusion $D(q) = P^\perp(q) + a(\xi(q))P(q)$, where $a : \xi(\mathcal{Q}) \rightarrow \mathbb{R}_+^*$ and P, P^\perp are defined in (8)-(9). Using Itô's lemma, it holds

$$\begin{aligned}
d\xi(q_t) &= [\nabla\xi(q_t) \cdot (-D(q_t)\nabla V(q_t) + \beta^{-1} \operatorname{div} D(q_t)) + \beta^{-1} D(q_t) : \nabla^2 \xi(q_t)] dt \\
&\quad + \sqrt{2\beta^{-1}} \nabla\xi(q_t) \cdot D(q_t)^{1/2} dW_t.
\end{aligned} \tag{53}$$

In view of (24), it holds

$$\nabla\xi(q) \cdot \operatorname{div} P(q) = \Delta\xi(q) - \frac{\nabla\xi(q)^\top \nabla^2 \xi(q) \nabla\xi(q)}{\|\nabla\xi(q)\|^2} = P^\perp(q) : \nabla^2 \xi(q). \tag{54}$$

Using the formula for the square root (23), along with (25), (10) and (54), the dynamics (53) simplifies as

$$\begin{aligned}
d\xi(q_t) &= \left(-a(\xi(q_t)) (\nabla V(q_t) \cdot \nabla\xi(q_t) - \beta^{-1} \Delta\xi(q_t)) + \beta^{-1} a'(\xi(q_t)) \|\nabla\xi(q_t)\|^2 \right) dt \\
&\quad + \sqrt{2\beta^{-1} a(\xi(q_t))} \nabla\xi(q_t) \cdot dW_t,
\end{aligned}$$

which is exactly (18). Using that a and a' are functions of $\xi(q) = z$, the conditional expectations of the drift and noise are given by

$$\begin{cases} b_a(z) = -a(z) \int_{\Sigma(z)} (\nabla V \cdot \nabla\xi - \beta^{-1} \Delta\xi) d\pi^\xi + \beta^{-1} a'(z) \int_{\Sigma(z)} \|\nabla\xi\|^2 d\pi^\xi, \\ \sigma_a^2(z) = a(z) \int_{\Sigma(z)} \|\nabla\xi\|^2 d\pi^\xi, \end{cases}$$

which is exactly (20). Lastly, (21) follows directly from (16). This concludes the proof.

7 Normalization constant of the diffusion

Let us first recall that the computation of the normalization constant of the diffusion is only for results to be comparable when performing numerical experiments. In practice, this normalization constant simply rescales the time step Δt . However, when performing simulations where the free energy is learned on the fly, computing this normalization constant is useful in order to prevent unstable dynamics due to large values of the diffusion.

We use the L^p normalization constraint (4) with $p = 1$ to compute the scalar κ_α in (12). The main motivation to use the L^p constraint is that, for the class of diffusions (12), it can be rewritten as an integral over the latent space, so that its computation is numerically tractable. The choice $p = 1$ is motivated by the fact that it does not require to estimate an additional conditional expectation.

Let us first give the conditioning formula between the two measures (6)-(13): for any test functions $f : \xi(\mathcal{Q}) \rightarrow \mathbb{R}$ and $g : \mathcal{Q} \rightarrow \mathbb{R}$,

$$\int_{\mathcal{Q}} f(\xi(q))g(q)Z^{-1}e^{-\beta V(q)}dq = \int_{\xi(\mathcal{Q})} f(z) \left(\int_{\Sigma(z)} g d\pi^\xi(\cdot|z) \right) e^{-\beta F(z)}dz. \quad (55)$$

Since the squared Frobenius norm of the diffusion (12), given by

$$|D_\alpha(q)|_{\mathbb{F}}^2 = \kappa_\alpha^2 ((d-1) + a_\alpha(\xi(q))^2),$$

is a function of $\xi(q)$, we can use the conditioning formula (55), to rewrite the L^p constraint (4) as

$$\begin{aligned} \int_{\mathcal{Q}} |D(q)|_{\mathbb{F}}^p e^{-\beta p V(q)} dq &= Z \int_{\mathcal{Q}} |D(q)|_{\mathbb{F}}^p e^{-\beta(p-1)V(q)} Z^{-1} e^{-\beta V(q)} dq \\ &= Z \kappa_\alpha^p \int_{\xi(\mathcal{Q})} ((d-1) + a_\alpha(z)^2)^{p/2} \left(\int_{\Sigma(z)} e^{-\beta(p-1)V} d\pi^\xi(\cdot|z) \right) e^{-\beta F(z)} dz. \end{aligned} \quad (56)$$

Choosing $p = 1$, the conditional measure on the right-hand side of (56) is simply equal to 1. Without loss of generality, we consider that $Z = 1$ (this can be achieved by adding a constant to the potential V), which does not alter the optimality of the homogenized diffusion (5). The only effect is potentially having a suboptimal multiplicative constant in factor of $e^{\alpha\beta F}$ when $\alpha = 1$ for the effective dynamics. The scalar κ_α is then given by (27).

Remark 5. *It is possible to use an L^p constraint with $p > 1$ by estimating the conditional measure on the right-hand side of (56), typically using ABF-like methods as described in Section 2.4 (which means that the normalizing constant can also be learned on the fly).*

8 Computations related to the numerical experiment

Derivatives of the collective variable ξ . The second derivatives write

$$\left\{ \begin{array}{l} \partial_{x_1}^2 \xi(q) = \frac{1}{2w \|q_2 - q_1\|} \left[1 - \frac{(x_1 - x_2)^2}{\|q_2 - q_1\|^2} \right], \\ \partial_{y_1}^2 \xi(q) = \frac{1}{2w \|q_2 - q_1\|} \left[1 - \frac{(y_1 - y_2)^2}{\|q_2 - q_1\|^2} \right], \\ \partial_{x_1, y_1}^2 \xi(q) = -\frac{1}{2w \|q_2 - q_1\|^3} (x_1 - x_2)(y_1 - y_2), \\ \partial_{x_1, x_2}^2 \xi(q) = -\partial_{x_2}^2 \xi(q) = -\partial_{x_1}^2 \xi(q), \\ \partial_{y_1, y_2}^2 \xi(q) = -\partial_{y_2}^2 \xi(q) = -\partial_{y_1}^2 \xi(q), \\ \partial_{y_2, x_1}^2 \xi(q) = \partial_{y_1, x_2}^2 \xi(q) = -\partial_{x_2, y_2}^2 \xi(q) = -\partial_{x_1, y_1}^2 \xi(q). \end{array} \right. \quad (57)$$

Computing the divergence of the diffusion matrix. Since $\|\nabla\xi\| = 1/(2w^2)$ is constant, we can use the simplified expressions for the divergence of Remark 2. Using the various relations between the first and second derivatives (see (31)-(57)), the expression of the divergence of the diffusion matrix (25) reduces to

$$\operatorname{div} D_\alpha(q) = 2w^2\kappa_\alpha \left[2 \left(2w^2 e^{\alpha\beta F \circ \xi(q)} - 1 \right) \left(\partial_{x_1}^2 \xi(q) + \partial_{y_1}^2 \xi(q) \right) + \alpha\beta F' \circ \xi(q) e^{\alpha\beta F \circ \xi(q)} \right] \nabla \xi(q). \quad (58)$$

In particular, it holds $[\operatorname{div} D_\alpha(q)]_3 = -[\operatorname{div} D_\alpha(q)]_1$ and $[\operatorname{div} D_\alpha(q)]_4 = -[\operatorname{div} D_\alpha(q)]_2$. Recall that we used the simplification $2w^2 \approx 1$ for our numerical experiments.

9 Thermodynamic integration

In this section, we briefly review thermodynamic integration, and describe how this was implemented to run the numerical experiment in Section 2.3. This section is based on [29, Chapter 3].

Thermodynamic integration is based on the following identity:

$$\forall z \in [z_{\min}, z_{\max}], \quad F(z) - F(z_{\min}) = \int_{z_{\min}}^z F'(y) dy, \quad (59)$$

where the mean force F' is defined in (17), and the values of z_{\min}, z_{\max} are set by the practitioner. Ideally, these values define an interval such that the typical values of the collective variable lie in it. The integral on the right-hand side of (59) is typically approximated by a left-Riemann rule, using a grid of N_z evenly spaced point in the interval $[z_{\min}, z_{\max}]$:

$$\int_{z_{\min}}^z F'(y) dy \approx \sum_{i=1}^{B(z)} F'(z^i) \Delta z, \quad z^i = z_{\min} + \left(i - \frac{1}{2} \right) \Delta z, \quad \Delta z = \frac{z_{\max} - z_{\min}}{N_z}, \quad (60)$$

where $B : [z_{\min}, z_{\max}] \rightarrow \{1, \dots, N_z\}$ outputs the bin number the value of the collective variable lies in:

$$B(z) = 1 + \left\lfloor \frac{z - z_{\min}}{\Delta z} \right\rfloor.$$

Let $1 \leq i \leq N_z$. To estimate one value $F'(z^i)$, we need to compute an expectation with respect to the conditional measure $\pi^\xi(dq|z^i)$ defined in (6). This measure rewrites

$$\pi^\xi(dq|z^i) = \frac{e^{-\beta V^\xi(q)} \sigma_{\Sigma(z^i)}(dq)}{\int_{\Sigma(z^i)} e^{-\beta V^\xi} d\sigma_{\Sigma(z^i)}}$$

where the modified potential V^ξ writes $V^\xi = V + \beta^{-1} \ln \|\nabla\xi\|$. We therefore need to sample the probability measure whose density is proportional to $e^{-\beta V^\xi}$ on $\Sigma(z^i)$. This can be done using trajectories of the projected dynamics

$$\begin{cases} dq_t = -\nabla V^\xi(q_t) dt + \sqrt{2\beta^{-1}} dW_t + \nabla \xi(q_t) d\lambda_t, \\ \text{with } (\lambda_t)_{t \geq 0} \text{ an adapted process such that } \xi(q_t) = z^i. \end{cases}$$

Here, the process $(\lambda_t)_{t \geq 0}$ acts as a Lagrange multiplier. This dynamics is integrated numerically with the following predictor-correct scheme: let $q^0 \in \Sigma(z^i)$ and for $n \geq 0$,

$$\begin{cases} q^{n+1} = q^n - \nabla V^\xi(q^n) \Delta t + \sqrt{2\beta^{-1} \Delta t} G^{n+1} + \nabla \xi(q^{n+1}) \Delta \lambda^{n+1}, \\ \xi(q^{n+1}) = z^i, \end{cases} \quad (61)$$

where $G^{n+1} \sim \mathcal{N}(0, I_d)$. The value of the Lagrange multiplier $\Delta \lambda^{n+1}$ is determined by the requirement that the constraint $\xi(q^{n+1}) = z^i$ is satisfied.

Computation of the Lagrange multiplier for the numerical example of Section 2.3.

Since $\|\nabla\xi\|$ is constant for our numerical experiment, we simply set $V^\xi = V$. In practice, the update (61) is performed by first computing the unconstrained move

$$\tilde{q}^{n+1} = q^n - \nabla V(q^n)\Delta t + \sqrt{2\beta^{-1}\Delta t}G^{n+1},$$

and then solving for $\Delta\lambda^{n+1}$. In view of (31), only the components of q^{n+1} corresponding to the dimer differ from the ones of \tilde{q}^{n+1} . Denote by $q_1, q_2 \in (\ell\mathbb{T})^2$ the positions of the particles composing the dimer. Then,

$$\begin{cases} q_1^{n+1} = \tilde{q}_1^{n+1} + \frac{q_1^{n+1} - q_2^{n+1}}{2w\|q_1^{n+1} - q_2^{n+1}\|}\Delta\lambda^{n+1}, \\ q_2^{n+1} = \tilde{q}_2^{n+1} - \frac{q_1^{n+1} - q_2^{n+1}}{2w\|q_1^{n+1} - q_2^{n+1}\|}\Delta\lambda^{n+1}. \end{cases} \quad (62)$$

Subtracting both equalities leads to

$$\left(1 - \frac{\Delta\lambda^{n+1}}{w\|q_1^{n+1} - q_2^{n+1}\|}\right)(q_2^{n+1} - q_1^{n+1}) = \tilde{q}_2^{n+1} - \tilde{q}_1^{n+1}. \quad (63)$$

From $\xi(q^{n+1}) = z^i$ it follows that $\|q_1^{n+1} - q_2^{n+1}\| = 2wz^i + r_0$. Taking the norm in (63) yields

$$|w(2wz^i + r_0) - \Delta\lambda^{n+1}| = w\|\tilde{q}_2^{n+1} - \tilde{q}_1^{n+1}\| = w(2w\xi(\tilde{q}^{n+1}) + r_0).$$

It follows that

$$\Delta\lambda^{n+1} = w(2wz^i + r_0) \pm w(2w\xi(\tilde{q}^{n+1}) + r_0).$$

We choose the solution with the minus sign as this choice leads to a consistent discretization in the limit $\Delta t \rightarrow 0$. Therefore, the Lagrange multiplier is equal to

$$\Delta\lambda^{n+1} = 2w^2(z^i - \xi(\tilde{q}^{n+1})).$$

Notice that, by adding the two equalities in (62), it holds $q_1^{n+1} + q_2^{n+1} = \tilde{q}_1^{n+1} + \tilde{q}_2^{n+1}$. Therefore, writing $q_1^{n+1} = (q_1^{n+1} + q_2^{n+1} - (q_2^{n+1} - q_1^{n+1}))/2$ (and similarly for q_2^{n+1}) and using (63) leads to

$$\begin{cases} q_1^{n+1} = \frac{1}{2}\left(1 + \frac{1}{1 - \frac{\Delta\lambda^{n+1}}{w(2wz^i + r_0)}}\right)\tilde{q}_1^{n+1} + \frac{1}{2}\left(1 - \frac{1}{1 - \frac{\Delta\lambda^{n+1}}{w(2wz^i + r_0)}}\right)\tilde{q}_2^{n+1}, \\ q_2^{n+1} = \frac{1}{2}\left(1 - \frac{1}{1 - \frac{\Delta\lambda^{n+1}}{w(2wz^i + r_0)}}\right)\tilde{q}_1^{n+1} + \frac{1}{2}\left(1 + \frac{1}{1 - \frac{\Delta\lambda^{n+1}}{w(2wz^i + r_0)}}\right)\tilde{q}_2^{n+1}. \end{cases} \quad (64)$$

Remark 6. Note that the update (64) is undefined when $\Delta\lambda^{n+1} = w(2wz^i + r_0)$. This corresponds to $\|\tilde{q}_2^{n+1} - \tilde{q}_1^{n+1}\| = 0$, which is not observed in practice due to the strong repulsive force when the distance goes to 0 (see (28)).

Respecting the periodic boundary conditions. Note that the norm $\|q_2 - q_1\|$ is computed taking the periodic boundary conditions into account. In practice, we first translate \tilde{q}_1^{n+1} to the frame of reference of \tilde{q}_2^{n+1} , apply the update, and periodize.

Hyperparameters for the numerical experiment. To obtain the mean force and free energy profiles to run the simulations in Section 2.3, we used $N_z = 100$ points in the interval $[z_{\min}, z_{\max}]$ (see (60)) and used a time step $\Delta t = 2.5 \times 10^{-5}$. The initial configuration for the first level $z^0 = z_{\min}$ is set to q^0 defined in (33) except for y_2^0 which is set to $y_1^0 + r_0 + 2wz_{\min}$ so that $\xi(q^0) = z_{\min}$. At the end of each simulation at the level z^i , the final configuration is changed so that it becomes the initial configuration for the simulation for the level z^{i+1} (i.e. we slightly move the second component of the second particle so that the new constraint is satisfied). The simulation for each level z^i was run for 125 units of time. The free energy is then reconstructed by integrating the mean force over the interval $[z_{\min}, z_{\max}]$.